JOURNAL OF COMPUTATIONAL PHYSICS 70, 463–499 (1987)

An Analysis of Time Discretization in the Finite Element Solution of Hyperbolic Problems

J. DONEA

Applied Mechanics Division, Joint Research Centre of the Commission of the European Communities, Ispra, Italy

L. QUARTAPELLE

Istituto di Fisica, Politecnico di Milano, Milano, Italy

AND

V. SELMIN

Applied Mechanics Division, Joint Research Centre of the Commission of the European Communities, Ispra, Italy

Received April 18, 1986; revised September 5, 1986

The problem of the time discretization of hyperbolic equations when finite elements are used to represent the spatial dependence is critically examined. A modified equation analysis reveals that the classical, second-order accurate, time-stepping algorithms, i.e., the Lax–Wendroff, leap-frog, and Crank–Nicolson methods, properly combine with piecewise linear finite elements in advection problems only for small values of the time step. On the contrary, as the Courant number increases, the numerical phase error does not decrease uniformly at all wavelengths so that the optimal stability limit and the unit CFL property are not achieved. These fundamental numerical properties can, however, be recovered, while still remaining in the standard Galerkin finite element setting, by increasing the order of accuracy of the time discretization. This is accomplished by exploiting the Taylor series expansion in the time increment up to the third order *before* performing the Galerkin spatial discretization using piecewise linear interpolations. As a result, it appears that the proper finite element equivalents of second-order finite difference schemes are implicit methods of incremental type having third- and fourth-order global accuracy on uniform meshes (Taylor–Galerkin methods). Numerical results for several linear examples are presented to illustrate the properties of the Taylor–Galerkin schemes in one- and two-dimensional calculations.

0021-9991/87 $3.00

0. INTRODUCTION

Most finite difference codes for computing transient flows and solving dynamical problems are based on second-order accurate time-stepping algorithms, namely, the Lax–Wendroff, leap-frog, and Crank–Nicolson schemes [1–4]. Due to its dissipative character, the Lax–Wendroff method has enjoyed wide-spread use in the analysis of nonlinear hyperbolic problems, where solutions are often characterized by the presence of strong gradients, such as shock waves and contact discontinuities. On the other hand, the leap-frog and Crank–Nicolson methods, which are marginally stable, are extensively used in the computation of smooth solutions to pure advection or wave propagation problems, as well as in situations governed by mixed advection–diffusion or pure diffusion.

Owing to their demonstrated effectiveness in finite difference computations, the above second-order time-stepping methods were largely used also in connection with finite element spatial discretizations of hyperbolic and parabolic problems (see, among others, [5–7]). One of the advantages of the conventional Galerkin finite element approach in the solution of the linear, one-dimensional, advection equation

$$u_t + au_x = 0, \qquad a = \text{constant}, \tag{0.1}$$

is that the discretization based on a uniform mesh of piecewise linear elements yields a fourth-order spatial accuracy for transient solutions, while the familiar central difference method is only second-order accurate in the mesh size [4, 5]. This result is illustrated in Fig. 1, where the phase velocity responses of the spatially discrete approximations to Eq. (0.1) resulting from central differences and from linear finite elements are compared. However, one eventually has to discretize in time, and the superior spatial accuracy of linear finite elements over central differences actually manifests itself only for small values of the time increment, i.e., only when the error due to the discrete time integration is negligible with respect to that caused by the spatial discretization. Now, computational efficiency clearly requires that time steps as large as possible be used in practical computations, particularly when finite elements are employed due to the presence of the consistent mass matrix

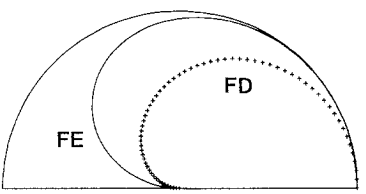

FIG. 1. Phase velocity response of semi-discrete approximations to the advection equation in one dimension. Comparison of spatial discretizations based on central finite differences (FD) and linear finite elements (FE).

in finite element equations for transient problems. Therefore, a basic issue concerning the use of finite elements in hyperbolic problems is the following: can the superior spatial accuracy of linear finite elements be fully exploited in practice, without being eroded by the error due to temporal discretization as the time step is increased? Answering this question is important also in a finite difference context since some high-order difference methods (e.g., the Padé rational approximations to spatial derivatives) lead to schemes very closely related to finite element schemes.

To our knowledge, Morton and Parrott [8] were the first to consider the problem of a proper coupling between the time discretization and the Galerkin spatial approximation of hyperbolic problems. They pointed out that several disadvantages of the Galerkin approach become apparent as soon as a standard, low-order, time discretization is introduced. In particular, a reduced stability range for schemes derived from explicit integrators is generally obtained as compared with the corresponding finite difference schemes. One of the consequences of this loss of stability is that the finite element schemes cannot be used when the Courant number approaches unity, while explicit finite difference schemes are exact in this limit. At the same time, this reduced stability range, which is directly related to the presence of a mass matrix in the Galerkin approach, is also accompanied by a rapid fall-off in the phase accuracy as the time step is increased. The approach adopted by Morton and Parrott to overcome the above difficulties was based on a Petrov–Galerkin formulation [8]. Special test functions were devised in one dimension with piecewise linear elements, with the objective of extending the stability and accuracy of pure Galerkin methods right up to the unit Courant number limit. However, the test functions introduced in the Petrov–Galerkin method for Euler, leap-frog, and Crank–Nicolson time-stepping do not retain all the valuable conservation properties associated with the pure Galerkin formulation, and the generalization of Petrov–Galerkin schemes to multidimensional and nonlinear problems faces some difficulties. An approach more closely based on the characteristics was subsequently elaborated upon by Morton [9]. This characteristic Galerkin method has been illustrated on a number of nonlinear test problems in one space dimension and appears very promising.

Another approach to developing time-accurate methods for the finite element solution of hyperbolic problems was suggested by the first author with the introduction of the Taylor–Galerkin method [10]. For the advection equation (0.1), the starting point is the substitution of space derivatives for time derivatives in a Taylor expansion, as used in the derivation of the Lax–Wendroff method, with the only modification that the procedure is carried out to the third order. On this basis, higher-order accurate versions of the Euler, leap-frog, Crank–Nicolson time-stepping algorithms were obtained. When combined with a conventional Galerkin spatial discretization, the resulting schemes were shown to possess the desired properties of extended stability and improved phase accuracy. Moreover, in contrast with the Petrov–Galerkin methods, schemes of Taylor–Galerkin type can be easily derived for nonlinear and multidimensional equations [10, 11], for hyperbolic systems [12, 13], and advection–diffusion problems [14].

The aim of the present paper is to provide a systematic analysis of the performances of both the standard, low-order, time-stepping methods and the improved Taylor–Galerkin schemes, when employed in the numerical solution of hyperbolic problems. The modified equation method of Warming and Hyett [15] is used as a basic tool for exposing the deficiencies of the standard time-stepping methods in a finite element context and revealing the necessary corrections which lead to the improved schemes of Taylor–Galerkin type.

An outline of the remainder of the paper follows: In Section 1, the modified equation method is briefly recalled to indicate how it can be applied to finite element equations. Sections 2–4 are devoted to the analysis of three basic time-stepping algorithms, namely, the single-step Lax–Wendroff method, the three-level leap-frog method, and the implicit Crank–Nicolson method, respectively. In each section, we successively analyze the finite difference and finite element schemes obtained by using second-order accurate time differencing, and the Taylor–Galerkin implicit scheme obtained by combining the improved time differencing algorithm with linear finite elements. The dispersion and dissipation properties of the various schemes are discussed qualitatively in terms of the truncation errors in the corresponding modified equations, and quantitatively in terms of relative phase errors and moduli of the amplification factors. Finally, Section 5 extends the previous analyses to the case of two-dimensional equations. Several numerical examples are presented which corroborate the theoretical analysis.

1. Modified Equation for Finite Element Schemes

In order to investigate and compare the numerical properties of the various schemes approximating the advection equation (0.1), the "modified equation method" of Warming and Hyett [15] will be employed. The *modified equation* is the actual partial differential equation which is solved numerically, apart from round-off errors, when a given finite difference scheme is applied to solve an initial value problem. The procedure to determine the modified equation requires some tedious algebra: the difference equation is first expanded in a double Taylor series in time and space and subsequently all the time derivatives except for the first-order one are then eliminated through the Taylor expanded equation (not the original differential equation) suitably differentiated. Fortunately, the entire procedure can be programmed on a computer using a symbolic manipulation language such as FORMAC [15] or REDUCE [16].

The terms appearing in the modified equation which are not in the original partial differential equation represent the truncation error of the numerical schemes. The main advantage of the approach is that these error terms provide immediate information about the dissipation and dispersion properties of the numerical scheme. In fact, the even and odd derivative terms are found to be associated, respectively, to amplitude and phase errors [15]. Also, a necessary condition for stability can be easily obtained simply by inspecting the sign of the coefficient of the

lowest order even-derivative term appearing in the modified equation. However, the von Neumann method, expressed either in the clasical way [1–3] or possibly according to the Schur–Cohn theory [17], must be employed to obtain a complete stability analysis.

The modified equation method, although originally formulated for finite difference schemes, can be applied also to the difference equations which result when finite elements are used to represent the spatial dependence. To give an idea of the simple modifications required with finite element equations, let the explicit Euler integration algorithm be applied to the advection equation (0.1), namely,

$$(u^{n+1}-u^n)/\Delta t = -au_x^n + O(\Delta t). \tag{1.1}$$

The solution $u(x)$ at each time level is then approximated by means of the expansion

$$U(x)=\sum_j U_j\phi_j(x), \tag{1.2}$$

where $\phi_j(x)$ is the "hat" function centred at the node x_j, and $\{U_j\}$ is the vector of nodal values. The fully discretized Galerkin equations are obtained by substituting expansion (1.2) into Eq. (1.1) and by taking the scalar product $\langle\ ,\ \rangle$ of the resulting equation with the same functions $\phi_j(x)$ used in the expansion (1.2). In the case of a uniform mesh of size h, one obtains

$$\begin{aligned}&[\tfrac{1}{6}(U_{j-1}^{n+1}+4U_j^{n+1}+U_{j+1}^{n+1})-\tfrac{1}{6}(U_{j-1}^n+4U_j^n+U_{j+1}^n)]/\Delta t\\ &\quad=-a(U_{j+1}^n-U_{j-1}^n)/2h.\end{aligned} \tag{1.3}$$

Note that the use of (linear) finite elements implies that the value of the spatial derivative at the jth node affects the temporal variation not only at this node but also at the two neighboring nodes $j\pm1$, so that, in contrast to finite differences, the finite element equations are always implicit even when an explicit time-stepping algorithm is employed. When Eq. (1.3) is written in a matrix notation, it assumes the form

$$M(U^{n+1}-U^n)=-\frac{a\,\Delta t}{h}AU^n, \tag{1.4}$$

where M is the so-called consistent mass matrix and A is the matrix corresponding to the first-order (spatial) derivative. To obtain the modified equation corresponding to the finite element scheme (1.3), the quantities $U_{j\pm1}^n$ and $U_{j\pm1}^{n+1}$ are first expanded in a double Taylor series around $U_j^n=u$, which gives

$$\begin{aligned}&\frac{\partial u}{\partial t}+\frac{1}{2}\Delta t\frac{\partial^2 u}{\partial t^2}+\frac{1}{6}(\Delta t)^2\frac{\partial^3 u}{\partial t^3}+\frac{1}{6}h^2\frac{\partial^3 u}{\partial t\,\partial x^2}\\ &\quad+\cdots=-a\left(\frac{\partial u}{\partial x}+\frac{1}{6}h^2\frac{\partial^3 u}{\partial x^3}+\cdots\right).\end{aligned} \tag{1.5}$$

(For notational simplicity, the symbol u is used to denote both the solution of the original differential equation and the unknown of the modified equation even though the two are distinct functions.) Expression (1.5) differs from the equation corresponding to the finite difference scheme by the presence of the mixed derivative $\frac{1}{6}h^2\,\partial^3 u/\partial t\,\partial^2 x$ on the left-hand side. The occurrence of such a term is due to the presence of the nondiagonal mass matrix in finite element schemes and is related to the aforementioned intrinsically implicit character of the finite element equations for evolution problems. The higher-order time and mixed space-time derivatives in Eq. (1.5) are then eliminated according to the standard procedure described in the original paper [15]. Table I shows the process of elimination for the scheme (1.3) based on the explicit Euler algorithm (EE) in time and linear finite elements (FE) in space leading to the modified equation

$$u_t + au_x = -\tfrac{1}{2}avhu_{xx} - \tfrac{1}{3}av^2h^2u_{xxx} + \cdots, \tag{1.6}$$

where $v = a\,\Delta t/h$ is the Courant number. The negative coefficient of u_{xx} immediately shows that the scheme (1.3) is unconditionally unstable, a result also provided by the examination of its amplification factor

$$G_{\mathrm{FE}}^{\mathrm{EE}}(\xi, v) = (1 - iv\sin\xi)/(1 - \tfrac{2}{3}\sin^2\tfrac{1}{2}\xi), \tag{1.7}$$

TABLE I

Procedure for Determining the Modified Equation of the Finite Element Explicit Euler Scheme

	$\frac{\partial u}{\partial t}$	$\frac{\partial u}{\partial x}$	$\frac{\partial^2 u}{\partial t^2}$	$\frac{\partial^2 u}{\partial t\,\partial x}$	$\frac{\partial^2 u}{\partial x^2}$	$\frac{\partial^3 u}{\partial t^3}$	$\frac{\partial^3 u}{\partial t^2\,\partial x}$	$\frac{\partial^3 u}{\partial t\,\partial x^2}$	$\frac{\partial^3 u}{\partial x^3}$
Coefficients of the equation	1	a	$\frac{\Delta t}{2}$	0	0	$\frac{\Delta t^2}{6}$	0	$\frac{h^2}{6}$	$\frac{ah^2}{6}$
$-\frac{\Delta t}{2}\frac{\partial}{\partial t}$ Eq.			$-\frac{\Delta t}{2}$	$-\frac{a\,\Delta t}{2}$	0	$-\frac{\Delta t^2}{4}$	0	0	0
$\frac{a\,\Delta t}{2}\frac{\partial}{\partial x}$ Eq.				$\frac{a\,\Delta t}{2}$	$\frac{a^2\,\Delta t}{2}$	0	$\frac{a\,\Delta t^2}{4}$	0	0
$\frac{\Delta t^2}{12}\frac{\partial^2}{\partial t^2}$ Eq.						$\frac{\Delta t^2}{12}$	$\frac{a\,\Delta t^2}{12}$	0	0
$-a\frac{\Delta t^2}{3}\frac{\partial^2}{\partial t\,\partial x}$ Eq.							$-\frac{a\,\Delta t^2}{3}$	$-\frac{a^2\,\Delta t^2}{3}$	0
$-\frac{h^2}{6}(1-2v^2)\frac{\partial^2}{\partial x^2}$ Eq.								$-\frac{h^2}{6}(1-2v^2)$	$-\frac{ah^2}{6}(1-2v^2)$
	1	a	0	0	$\frac{a^2\,\Delta t}{2}$	0	0	0	$\frac{1}{3}ah^2v^2$

$$u_t + au_x = -\tfrac{1}{2}avhu_{xx} - \tfrac{1}{3}av^2h^2u_{xxx} + \cdots$$

where ξ is the dimensionless wave number, $0 \leqslant \xi \leqslant \pi$. The spatial discretizations provided by finite elements and differences can be compared by confronting the modified equation (1.6) with the modified equation associated with the standard finite difference explicit scheme, namely,

$$u_t + au_x = -\tfrac{1}{2}avhu_{xx} - \tfrac{1}{6}ah^2(1+2v^2)\,u_{xxx} + \cdots. \tag{1.8}$$

Therefore, using linear finite elements instead of finite differences leaves unchanged the temporal part of the truncation error (the terms depending on v) whereas it eliminates the contribution to the leading dispersion error due to the spatial discretization (the 1 within the brackets in Eq. (1.8)). This very simple and rather obvious result is important since it also holds in the case of the three second-order accurate time integrators which will be discussed in the following sections.

2. Lax–Wendroff Schemes

In order to eliminate the unconditional instability of the explicit Euler scheme (cf. the modified equation (1.8)), Lax and Wendroff have derived a finite difference (FD) scheme [18] by considering the Taylor series expansion in the time step Δt,

$$u^{n+1} = u^n + \Delta t\, u_t^n + \tfrac{1}{2}(\Delta t)^2\, u_{tt}^n + O[(\Delta t)^3]. \tag{2.1}$$

By substituting the advection equation $u_t = -au_x$ and $u_{tt} = a^2 u_{xx}$, Eq. (2.1) becomes

$$u^{n+1} = u^n - \Delta t a u_x^n + \tfrac{1}{2}(\Delta t)^2 a^2 u_{xx}^n + O[(\Delta t)^3]. \tag{2.2}$$

2.1. *Finite Differences*

When u_x and u_{xx} are replaced by standard second-order accurate central differences, namely,

$$(u_x)_j = h^{-1}(\Delta_0 U)_j = h^{-1}\tfrac{1}{2}(U_{j+1} - U_{j-1})$$

and

$$(u_{xx})_j = h^{-2}(\delta^2 U)_j = h^{-2}(U_{j-1} - 2U_j + U_{j+1}),$$

the well-known single-step Lax–Wendroff (LW) scheme is obtained

$$U^{n+1} = U^n - v\,\Delta_0 U^n + \tfrac{1}{2}v^2\,\delta^2 U^n. \tag{2.3}$$

The modified equation for this scheme is reported as the first line of Table II. The Warming and Hyett necessary condition for stability is seen to be $v^2 \leqslant 1$ and the leading terms of the truncation error vanish for $v = 1$. The examination of the amplification factor

$$G_{\mathrm{FD}}^{\mathrm{LW}}(\xi, v) = 1 - v^2(1 - \cos\xi) - iv \sin\xi \tag{2.4}$$

TABLE II

Modified Equations for the Schemes of Lax–Wendroff Type

Finite differences

$$u_t + au_x = -\tfrac{1}{6}ah^2(1-v^2)\,u_{xxx} - \tfrac{1}{8}ah^3v(1-v^2)\,u_{xxxx} - \tfrac{1}{120}ah^4(1+5v^2-6v^4)\,u_{xxxxx} + \cdots$$

Finite elements

$$u_t + au_x = +\tfrac{1}{6}ah^2v^2u_{xxx} - \tfrac{1}{24}ah^3v(1-3v^2)\,u_{xxxx} + \tfrac{1}{180}\,ah^4(1-\tfrac{15}{2}v^2+9v^4)\,u_{xxxxx} + \cdots$$

Taylor–Galerkin (finite elements)

$$u_t + au_x = -\tfrac{1}{24}ah^3v(1-v^2)\,u_{xxxx} + \tfrac{1}{180}ah^4(1-5v^2+4v^4)\,u_{xxxxx} + \cdots$$

makes the picture of the scheme complete: the condition $v^2 \leqslant 1$ is also sufficient for stability and, since $G_{\mathrm{FD}}^{\mathrm{LW}}(\xi, v=1) = e^{-i\xi}$, the scheme satisfies the unit CFL condition. The relative phase error $\phi/\phi^{\mathrm{ex}} = \phi/(-v\xi) = \arg(G)/(-v\xi)$ and the modulus $|G|$ of the amplification factor of the Lax–Wendroff finite difference scheme are plotted in the polar diagrams of Fig. 2.1 for several values of v. As is well known, the scheme has a predominantly lagging phase error except for large wavenumbers when $v > \frac{1}{2}$. The scheme is dissipative especially at small wavelengths and for $v \sim \frac{1}{2}$. The dissipative character of the scheme leads sometimes to the interpretation of the second-order derivative appearing in Eq. (2.2) as an implicit numerical diffusion or viscosity inherent to the Lax–Wendroff method. It must be stressed, however, that, as far as time-dependent solutions are concerned, such an interpretation is erroneous since the second derivative term is only an element of the improved difference approximation to the time derivative with respect to the explicit Euler algorithm. Rather, the correction term is introduced by the Taylor series to counterbalance in the transient the *negative* diffusion intrinsic to the explicit Euler-stepping which makes such a scheme unstable for the advection equation. From this viewpoint, the use of the Taylor series (2.1) in the Lax–Wendroff method [illegible]

in conjunction with any method of spatial discretization.

2.2. *Finite Elements*

If the piecewise linear representation (1.2) is assumed for the unknown $u(x)$, the Lax–Wendroff finite element scheme (LWFE),

$$[1 + \tfrac{1}{6}\delta^2](U^{n+1} - U^n) = -v\,\Delta_0 U^n + \tfrac{1}{2}v^2\,\delta^2 U^n, \tag{2.5}$$

is obtained and the amplification factor assumes the form

$$G_{\mathrm{FE}}^{\mathrm{LW}}(\xi, v) = 1 - (2v^2 \sin^2 \tfrac{1}{2}\xi + iv \sin \xi)/(1 - \tfrac{2}{3}\sin^2 \tfrac{1}{2}\xi). \tag{2.6}$$

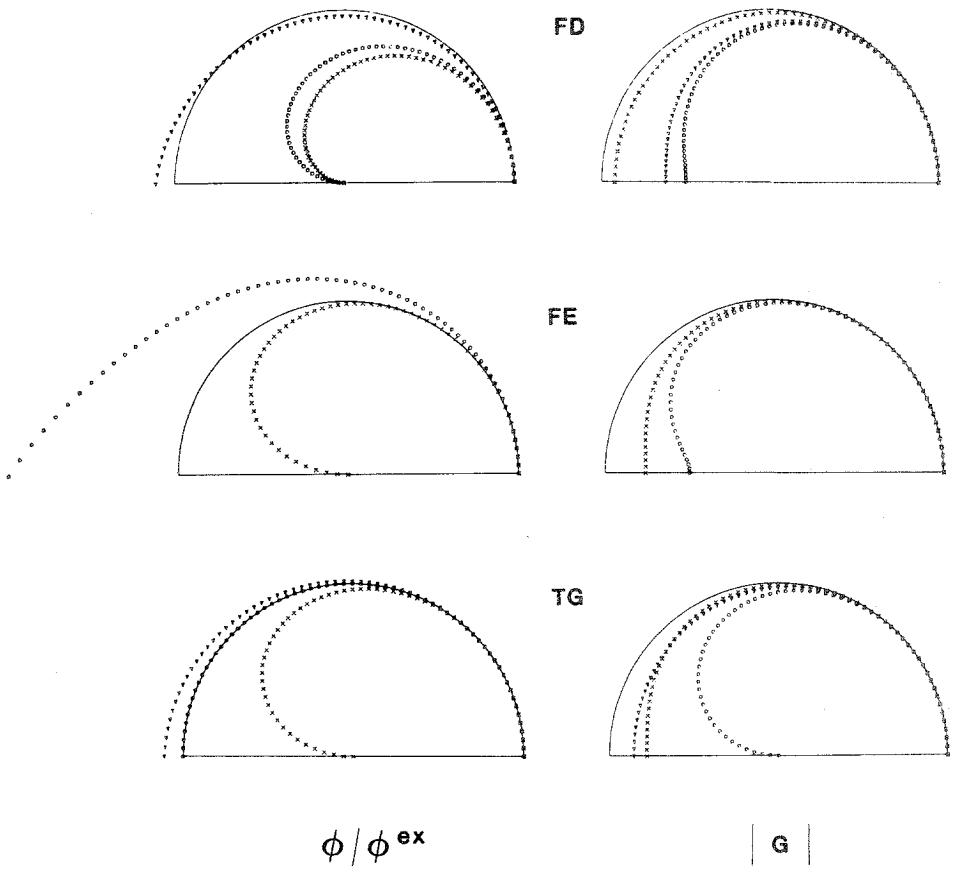

FIG. 2.1. Relative phase error ϕ^{LW}/ϕ^{ex} (left) and amplification factor modulus $|G^{LW}|$ (right) of the Lax–Wendroff schemes. (×) $\nu = 0.2$, (○) $\nu = 0.5$, and (▽) $\nu = 0.9$.

The modified equation of this finite element scheme is shown in Table II for comparison with the original finite difference scheme. The spatial discretization is seen not to contribute to the (leading) dispersion error. On the other hand, using a linear interpolation affects the dissipation error and reduces the domain of numerical stability ($\nu^2 < \frac{1}{3}$) with respect to the finite difference scheme. By examining the curves of the relative phase error plotted in Fig. 2.1, one sees that the higher-order phase accuracy of finite elements over finite differences is adequately exploited only for small Δt (cf. Fig. 1), whereas the phase error becomes positive and increases at intermediate and short wavelengths as $\nu^2 \to \frac{1}{3}$. Thus, the simple juxtaposition of the Lax–Wendroff time differencing and the piecewise linear finite element spatial approximation provides a scheme which can attain neither the unit CFL property nor the optimal stability limit $\nu^2 \leqslant 1$ typical of explicit finite difference schemes.

2.3. *Taylor–Galerkin*

The second modified equation in Table II indicates that the leading truncation error in the finite element scheme can be eliminated simply by going a step further in the Taylor series expansion (2.1), i.e., by including the third-order term as [10],

$$u^{n+1} = u^n + \Delta t u_t^n + \tfrac{1}{2}(\Delta t)^2 u_{tt}^n + \tfrac{1}{6}(\Delta t)^3 u_{ttt}^n + O[(\Delta t)^4]. \tag{2.7}$$

Then, the third-order derivative term is approximated in a mixed spatial–temporal form $u_{ttt} = (u_{tt})_t = (a^2 u_{xx})_t = a^2 u_{txx}$, so that Eq. (2.7) becomes

$$u^{n+1} = u^n - \Delta t a u_x^n + \tfrac{1}{2}(\Delta t)^2 a^2 u_{xx}^n + \tfrac{1}{6}(\Delta t)^3 a^2 u_{txx}^n + O[(\Delta t)^4]. \tag{2.8}$$

It is important to note that the presence of a third-order spatial derivative would prevent the use of finite elements with C_0 continuity for the spatial discretization, whereas the adopted mixed form leads to a simple modification of the usual consistent mass matrix. In fact, by substituting $u_t^n = (u^{n+1} - u^n)/\Delta t + O(\Delta t)$ into Eq. (2.8), a third-order accurate generalization of the Lax–Wendroff time differencing is obtained

$$[1 - \tfrac{1}{6}(\Delta t)^2 a^2 \partial_x^2](u^{n+1} - u^n)/\Delta t = -a u_x^n + \tfrac{1}{2} \Delta t a^2 u_{xx}^n. \tag{2.9}$$

The spatial discretization of Eq. (2.9) by means of the weak Galerkin formulation and using linear finite elements provides the implicit scheme [10],

$$[1 + \tfrac{1}{6}(1 - \nu^2)\, \delta^2](U^{n+1} - U^n) = -\nu\, \Delta_0 U^n + \tfrac{1}{2}\nu^2\, \delta^2 U^n. \tag{2.10}$$

The finite element scheme (2.10) based on the Taylor series including the third-order term will be called Lax–Wendroff Taylor–Galerkin (LWTG) to distinguish it from the second-order finite element scheme (2.5). (In Ref. [10] the scheme (2.10) was named Euler–Taylor–Galerkin to stress its derivation from the Euler time-stepping algorithm.) The only difference between the two finite element schemes is in the implicit operator in the term on the left-hand side of Eqs. (2.5) and (2.10). The third-order accuracy is obtained by a simple modification of the consistent mass matrix, the system of equations (2.10) remaining tridiagonal. The scheme being compact, no particular difficulty is met in the treatment of boundary conditions. Furthermore, the generalized consistent mass matrix is still symmetric. The modified equation corresponding to the scheme (2.10) is given in the last line of Table II. By comparing it with the lower-order finite element scheme, one notes that the leading dispersion error due to the time discretization has gone from the third- to the fifth-order derivative thanks to the higher time accuracy. Thus, going from finite differences to Taylor–Galerkin finite elements, one improves the phase accuracy because the use of finite elements and the inclusion of an additional term in the Taylor series eliminate the leading dispersion errors resulting from the spatial and temporal discretizations, respectively. The leading term of the dissipation error provides the necessary condition for numerical stability: $\nu^2 \leqslant 1$. Moreover, the

lowest order term of both dispersion and dissipation errors for the Lax–Wendroff Taylor–Galerkin scheme are found to be zero for $v^2 = 1$. These results are confirmed by examining the amplification factor of this scheme

$$G_{TG}^{LW}(\xi, v) = 1 - (2v^2 \sin^2 \tfrac{1}{2}\xi + iv \sin \xi)/(1 - \tfrac{2}{3}(1 - v^2) \sin^2 \tfrac{1}{2}\xi) \tag{2.11}$$

which gives the sufficient stability condition $v^2 \leqslant 1$ and shows that $G_{TG}^{LW}(\xi, v) = e^{-i\xi}$ for $v = 1$. Thus, the optimal stability limit and the unit CFL property are attained by the Taylor–Galerkin scheme. Furthermore, since $\phi_{TG}^{LW}/\phi^{ex} = 1$ also for $v = \frac{1}{2}$, the method has no phase error at all wavelengths for two distinct values of the Courant number but no dissipation error only for $v = 1$. The relative phase error and the modulus of the amplification factor of the LWTG scheme are shown in Fig. 2.1 which gives a complete picture of its superior phase accuracy with respect to the finite difference method. The phase error of the Taylor–Galerkin scheme is negative for $v < \frac{1}{2}$ and positive for $v > \frac{1}{2}$ at all wavelengths and the maximum dissipation occurs for $v = \frac{1}{2}$ when the phase of the scheme is exact.

It can be noted that the LWTG scheme can also be interpreted as a Petrov–Galerkin-like method. In fact, the standard Galerkin weak form of Eq. (2.9) provides, after integrating by parts the second-order derivatives and omitting the boundary terms for simplicity,

$$\langle [\phi_j + \tfrac{1}{6}(\Delta t)^2 a^2 \phi_j' \partial_x], (u^{n+1} - u^n) \rangle / \Delta t = -\langle \bar{\phi}_j, a u_x \rangle, \tag{2.12}$$

where

$$\bar{\phi}_j = \phi_j + \tfrac{1}{2} \Delta t \; a \, d\phi_j/dx \tag{2.12'}$$

is a modified weighting function. An advantage of the present Taylor–Galerkin (TG) approach over Petrov–Galerkin methods [8, 9] and [19–22] is that it does not involve any adjustable parameter to maximize the accuracy. Examination of Eqs. (2.12) shows that the weighting of the time-dependent term is different from that of the steady-state part of the equation: in other words, the present approach provides weak equations which are not in the consistent form typical of the Petrov–Galerkin methods wherein the spatial discretization precedes the time discretization [19–22]. In fact, the weighting of the transient term is fundamentally different in the two approaches. In the TG method the modified weighting results from, and is dictated by, the analysis of the truncation error of the time-stepping algorithm for the transient equation. On the contrary, in consistent Petrov–Galerkin methods for advection–diffusion or hyperbolic problems a modified weighting function is first formulated for the steady-state equation [20, 21] or for the time-continuous evolution equation [22] and only subsequently is it applied to all terms of the time-dependent equation or to a time discretized version of the latter.

On the other hand, the present approach has a stronger relationship with Petrov–Galerkin methods of characteristic type as developed by Morton and

Parrott [8] and the characteristic Galerkin method of Morton [9]. In fact, these methods are derived starting directly from time-discretized versions of the hyperbolic equations so that different weighting functions are derived for each time integration algorithm. In particular, the LWTG scheme (2.10) or (2.12) is found to be identical to the Euler–Petrov–Galerkin (EPGII) scheme [8] when the latter is operated at the optimal value of its adjustable parameter. Furthermore, the TG scheme provides a convenient approximation to the more general characteristic Galerkin method (see [9]). Galerkin methods of characteristic type thus allow the interpretation of the LWTG scheme as a third order characteristic method much in the same manner as the Leith scheme (see [2, pp. 75–77]) gives the interpretation of the Lax–Wendroff finite difference scheme as a characteristic method of second order accuracy for time-dependent solutions. In fact, at two successive time levels, the solutions denoted by $u^n(x)$ and $u^{n+1}(x)$ satisfy the characteristic relation

$$u^{n+1}(x) = u^n(x - a\,\Delta t),$$

which through a Taylor expansion yields

$$u^{n+1} = u^n - a\,\Delta t u_x^n + \tfrac{1}{2}(a\,\Delta t)^2\, u_{xx}^n - \tfrac{1}{6}(a\,\Delta t)^3\, u_{xxx}^n + O[(\Delta t)^4].$$

In view of the governing equation $u_t = -au_x$, this relation is clearly equivalent to Eq. (2.7), showing that the TG method is indeed a characteristic finite element method.

To illustrate and compare the performances of the three Lax–Wendroff schemes discussed so far, consider the advection problem over the spatial interval [0, 1] and defined by the initial and boundary conditions

$$\begin{aligned} u(x,0) &= \begin{cases} \tfrac{1}{2}\{1 + \cos[\pi(x - x_0)/\sigma]\} & \text{if } |x - x_0| \leqslant \sigma \\ 0 & \text{if } |x - x_0| > \sigma \end{cases} \\ u(0,t) &= 0, \qquad t \geqslant 0, \end{aligned} \tag{2.13}$$

with $x_0 = 0.2$ and $\sigma = 0.12$. The exact solution of Eq. (0.1) with $a = 1$ corresponds to the translation to the right of the initial profile with a unit velocity. Figure 2.2 compares the numerical solutions obtained using a uniform mesh of 50 elements and different values of ν with the exact solution at $t = 0.6$. Both schemes using finite elements display a greater phase accuracy than the finite difference scheme. However, the most simple LWFE scheme cannot be operated when $\nu^2 > \frac{1}{3}$ and displays an appreciable phase lead for $\nu \geqslant \frac{1}{2}$ (cf. the relative phase error in Fig. 2.1). The phase accuracy of the LWTG scheme is on the contrary rather uniform over the entire interval $0 < \nu < 1$. One can note that the maximum of the numerical solution for $\nu = \frac{1}{2}$ is slightly smaller than the exact value, in accordance with the fact that the amplitude error is a maximum for $\nu = \frac{1}{2}$ (cf. the amplification factor of LWTG in Fig. 2.1).

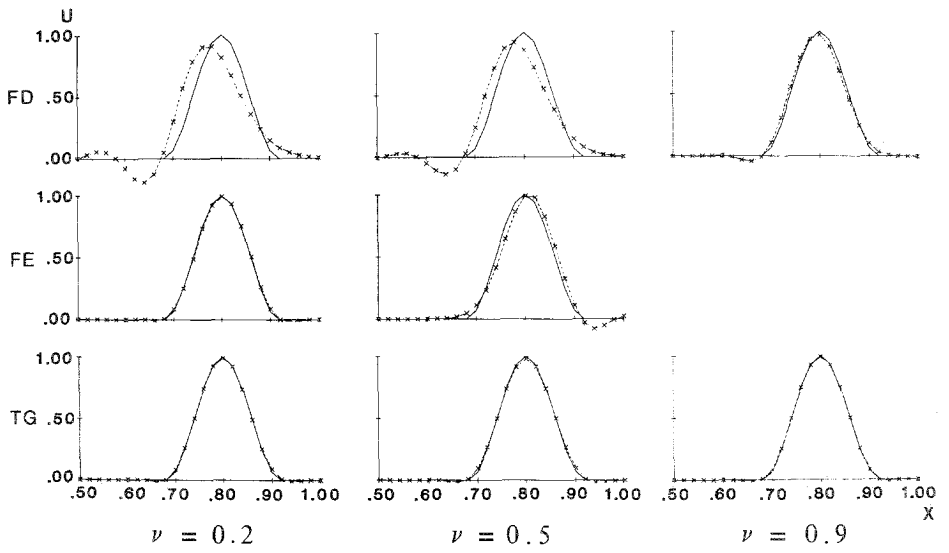

FIG. 2.2. Propagation of a cosine profile. Comparison of the Lax–Wendroff schemes for several values of the Courant number.

To be fair, it should be noted that the improved accuracy of the schemes based on finite elements with respect to the finite difference method has been obtained at the expense of making the schemes implicit: the solution of a system of linear equations is required at each time level. However, this is not a major difficulty insofar as approximate factorization techniques can be used with converge within the requested accuracy in a few iterations (see, e.g., [14]). Nevertheless, the fact remains that the finite elements introduce an implicitness into the equations while the scheme is only conditionally stable. Therefore, the LWTG scheme can provide very accurate solutions of truly transient problems but is to be considered as not particularly suited to compute steady-state solutions of stiff problems.

2.4. *Systems of Equations*

The LWTG scheme can also be used to solve systems of hyperbolic equations. To give a direct idea of such an extension, consider the linear wave equation

$$\psi_{tt} = a^2 \psi_{xx}, \qquad a = \text{constant}. \tag{2.14}$$

With the introduction of the auxiliary variables $v = \psi_t$ and $w = -a\psi_x$, one can solve it as a system of two first-order hyperbolic equations

$$\begin{aligned} v_t &= -aw_x, \\ w_t &= -av_x. \end{aligned} \tag{2.15}$$

System (2.15) is rewritten in vector form as

$$u_t = -aAu_x, \tag{2.16}$$

where

$$u = \begin{bmatrix} v \\ w \end{bmatrix} \quad \text{and} \quad A = \begin{bmatrix} 0 & 1 \\ 1 & 0 \end{bmatrix}. \tag{2.17}$$

The vector equivalent of the LWTG scheme (2.10) is easily found to be

$$[I + \tfrac{1}{6}(I - \nu^2 A^2)\,\delta^2](U^{n+1} - U^n) = -\nu A\, \Delta_0 U^n + \tfrac{1}{2}\nu^2 A^2\, \delta^2 U^n, \tag{2.18}$$

where I is the 2×2 identity matrix and $U = (V, W) = (\{V_j\}, \{W_j\})$. Note that, by virtue of (2.17), for the particular system (2.15), $A^2 = I$. Therefore, the correction term proportional to ν^2 in Eq. (2.18) does not couple the two unknowns v and w, and the solution of Eq. (2.18) requires two inversions of the same tridiagonal matrix. In more general cases, the matrix A^2 is not diagonal and a 2×2 block tridiagonal matrix must be inverted. In Figs. 2.3 and 2.4 the numerical solutions for

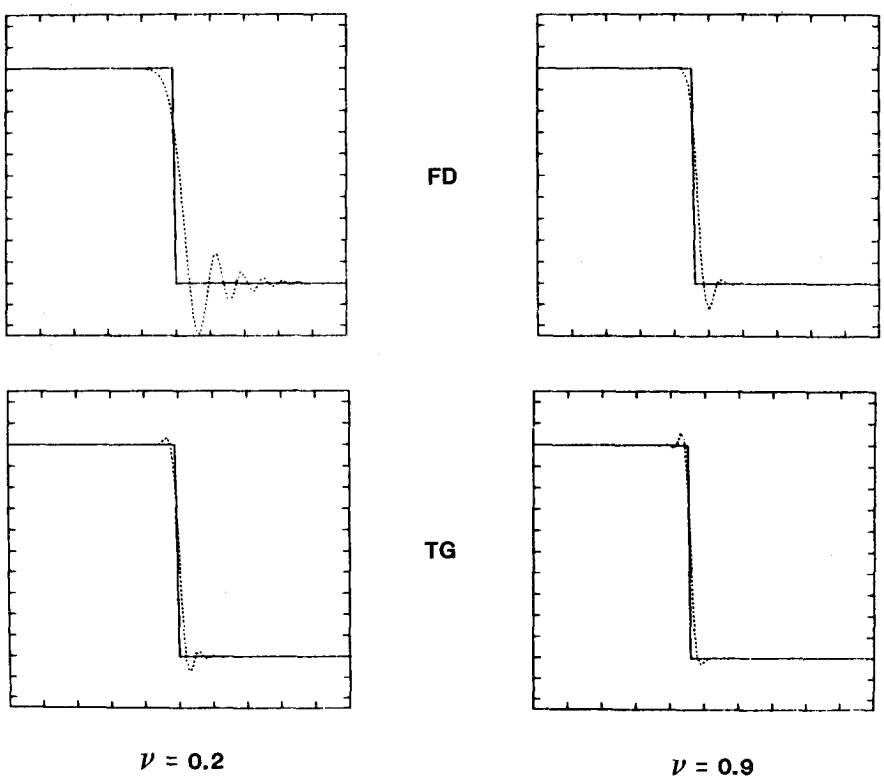

FIG. 2.3. Propagation of a compression wave in an elastic rod. Comparison of the velocity profiles computed by means of Lax–Wendroff schemes.

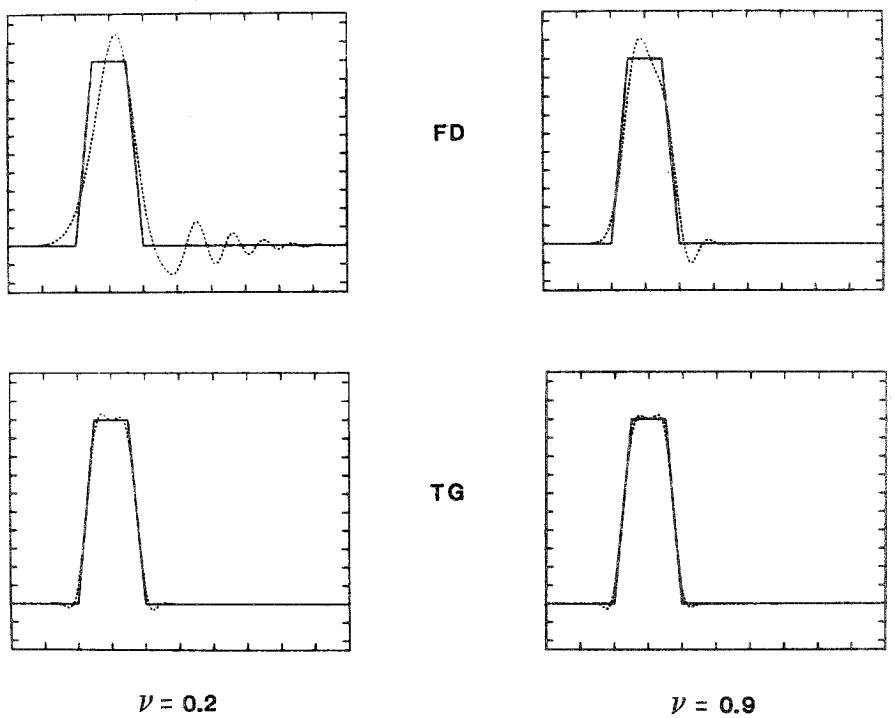

FIG. 2.4. Pressure pulse propagating in an elastic rod after one reflection at the free end. Comparison of the pressure profiles computed by means of Lax–Wendroff schemes.

two test problems calculated using the LWTG scheme (Eq. (2.18)) and the LWFD scheme (Eq. (2.18) with the implicit part dropped) are shown and compared to the exact solutions. The first test problem is the propagation of a discontinuous compression wave (for details see [13]). The results in Fig. 2.3 clearly confirm the excellent phase characteristics of the Taylor–Galerkin scheme with respect to the finite difference scheme. The second test problem is the reflection of a trapezoidal pressure pulse which propagates in a rod clamped at its end [13]. The reflected pressure pulse calculated by the two schemes is shown in Fig. 2.4. Here again, the numerical results are found to be in conformity with the phase and damping characteristics of the schemes. It should be emphasized that the TG scheme provides these good results without the complication associated with the decomposition into characteristic fields, which is present in many other numerical methods. For a Taylor–Galerkin scheme formulated directly for the second-order hyperbolic equation (2.14) see Ref. [13].

The two LW schemes using finite elements can also be extended to deal with nonlinear systems of hyperbolic equations. This is illustrated in Fig. 2.5 which shows the solutions extracted from [12] of a Riemann problem for a perfect gas—the well-known Sod shock-tube problem. The calculations have been performed

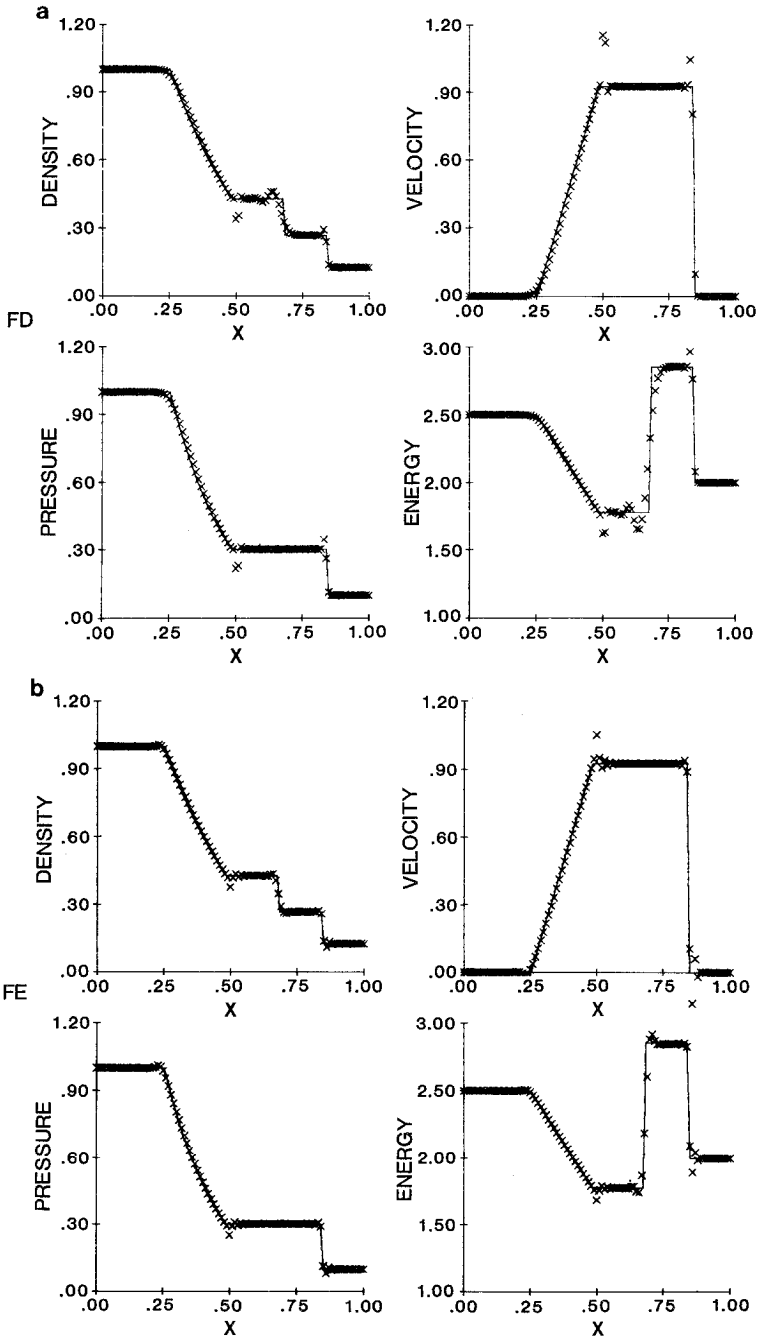

FIG. 2.5. Numerical solutions to the Sod shock-tube problem obtained by means of nonlinear Lax–Wendroff schemes. Comparison of (a) two-step finite difference scheme ($\nu = 0.9$), (b) second-order finite element scheme ($\nu = 0.45$), and (c) third-order Taylor–Galerkin scheme ($\nu = 0.9$).

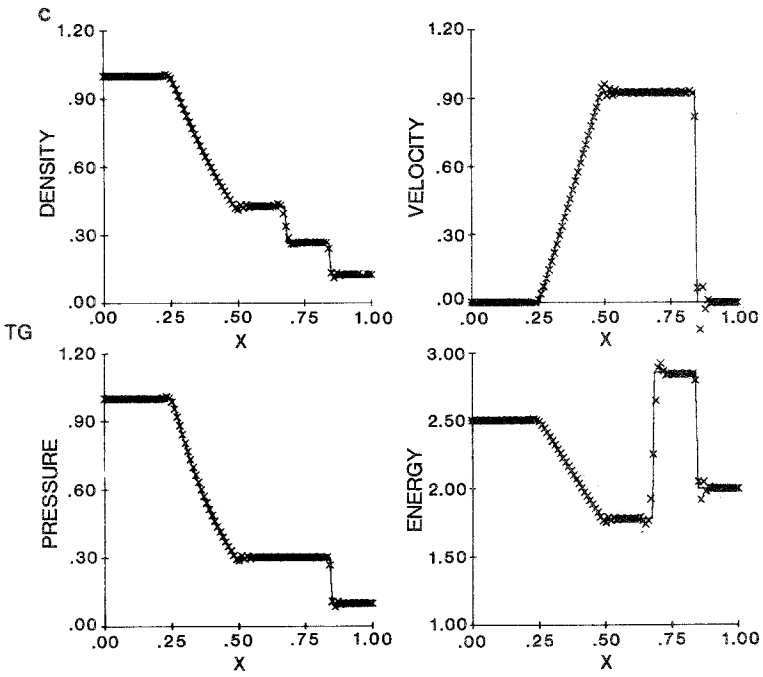

FIG. 2.5—*Continued.*

on a uniform mesh using a time step corresponding to a CFL condition number of 0.9 for the explicit, two-step, Lax–Wendroff finite difference scheme and the Taylor–Galerkin scheme, whereas a CFL number of 0.45 was employed for the

[redacted]

employed in compression regions (for details see [11]). The comparison of the results in Fig. 2.5 shows the superiority of the finite element schemes which manifests itself by a better overall accuracy, a much reduced amplitude of non-physical oscillations and a sharper representation of the discontinuities.

3. LEAP-FROG SCHEMES

As shown in [10], a generalized leap-frog time-stepping algorithm can be derived in the form

$$[1 - \tfrac{1}{6}(\Delta t)^2 a^2 \partial_x^2](u^{n+1} - u^{n-1})/2\,\Delta t = -au_x^n. \tag{3.1}$$

On a uniform mesh of linear elements the specific form of the leap-frog Taylor–Galerkin scheme (LFTG) is

$$[1 + \tfrac{1}{6}(1 - \nu^2)\,\delta^2](U^{n+1} - U^{n-1}) = -2\nu\,\Delta_0 U^n. \tag{3.2}$$

TABLE III

Modified Equations for the Schemes of Leap-Frog Type

Finite differences
$u_t + au_x = -\frac{1}{6}ah^2(1-v^2)\,u_{xxx} + \frac{1}{120}ah^4(1-10v^2+9v^4)\,u_{xxxxx} + \cdots$
Finite elements
$u_t + au_x = \frac{1}{6}ah^2v^2u_{xxx} + \cdots$
Taylor–Galerkin (finite elements)
$u_t + au_x = \frac{1}{360}ah^4(2+5v^2-7v^4)\,u_{xxxxx} + \cdots$

This scheme is fourth-order accurate and its stability condition reads $v^2 \leqslant 1$, while the standard LFFE scheme has the reduced stability limit $v^2 \leqslant \frac{1}{3}$. Scheme (3.2) was obtained by Morton and Parrott [8], using a Petrov–Galerkin approach of characteristic type and choosing the optimal value of the adjustable parameter therein available.

The modified equation associated with Eq. (3.2) is shown in Table III together with those corresponding to the finite difference leap-frog scheme [23, 24] and the standard LFFE scheme. The improved phase accuracy of the TG scheme is clearly apparent from the fact that the leading truncation error is now in terms of a fifth-order spatial derivative, in contrast to the third derivative appearing in the classical schemes. This is confirmed by the polar diagrams of the relative phase error in Fig. 3.1. It is important to note that both the finite difference scheme and the

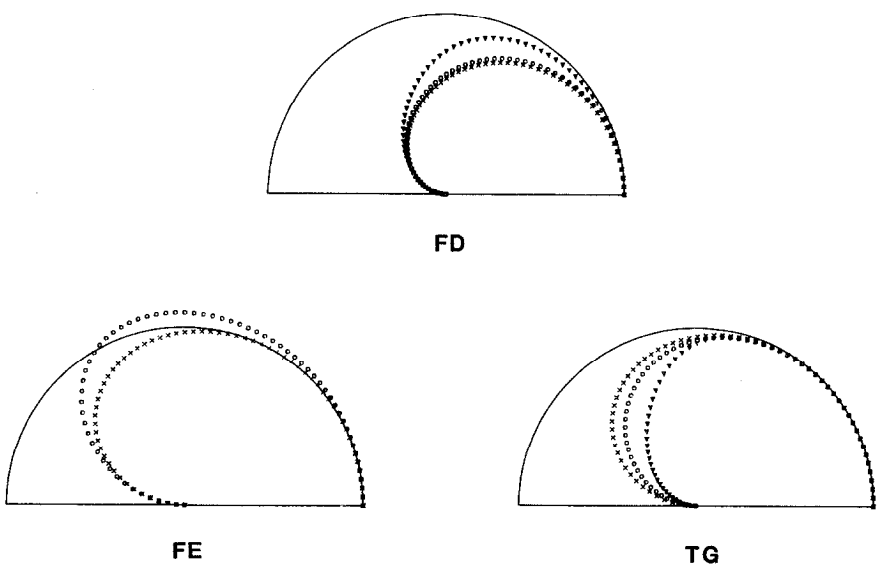

Fig. 3.1. Relative phase error ϕ^{LF}/ϕ^{ex} of the leap-frog schemes (×) $v = 0.2$, (○) $v = 0.5$, (▽) $v = 0.9$.

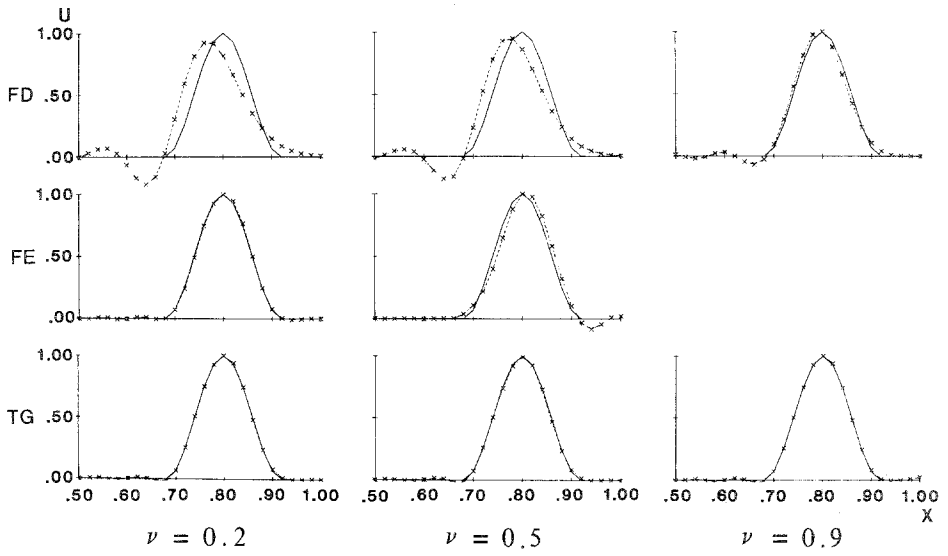

FIG. 3.2. Propagation of a cosine profile. Comparison of leap-frog schemes for several values of the Courant number.

Taylor–Galerkin scheme satisfy the unit CFL property only within a limited range of wavelengths. In fact it can be shown that $\phi^{LF}/\phi^{ex} = 1$ at $\nu = 1$ only for $0 \leqslant \xi \leqslant \pi/2$, whereas $\phi^{LF}/\phi^{ex} < 1$ for $\pi/2 \leqslant \xi \leqslant \pi$ (see also [4, p. 60], for the finite difference case). Therefore, these leap-frog schemes operated with $\nu = 1$ provide the exact solution only for signals with wavelength $\lambda = 2\pi/(\xi/h) = 2\pi h/\xi$ such that $4h \leqslant \lambda < \infty$ whereas the short wavelengths in the range $2h < \lambda < 4h$ propagate with a wrong speed. This result is a direct consequence of the three-level character of the leap-frog time differencing. The numerical behaviour of the three leap-frog schemes is illustrated in Fig. 3.2 which shows the solutions of the test problem (2.13) for different values of ν.

4. CRANK–NICOLSON SCHEMES

A similar analysis can be performed in the case of the Crank–Nicolson (CN) time-stepping algorithm. Considering forward and backward Taylor series expansions extended up to the fourth-order term [10], a generalization of the Crank–Nicolson algorithm is obtained in the so-called incremental (delta) form [25],

$$[1 + \tfrac{1}{2}\Delta t a\,\partial_x + \tfrac{1}{12}(\Delta t)^2 a^2\,\partial_x^2](u^{n+1} - u^n)/\Delta t = -a u_x^n. \tag{4.1}$$

The spatial approximation of Eq. (4.1) by means of linear finite elements gives the CNTG scheme

$$[1+\tfrac{1}{6}(1+\tfrac{1}{2}v^2)\,\delta^2+\tfrac{1}{2}v\,\Delta_0](U^{n+1}-U^n)=-v\,\Delta_0 U^n. \tag{4.2}$$

The CNTG scheme (4.2) is nondissipative as opposed to the third-order Crank–Nicolson Petrov–Galerkin scheme developed in [8]. Scheme (4.2) has also been obtained by Harten and Tal-Ezer by combining the fourth-order time discretization (4.1) with a fourth-order accurate Padé approximation of the spatial derivative [26, 27]. The same scheme has also been considered in [28] as a particular case of Padé schemes with maximum order of accuracy.

The modified equations of the standard Crank–Nicolson schemes and of its TG version are reported in Table IV. Since the coefficients of the leading error terms of the finite difference scheme are always positive, the unit CFL property cannot be attained when the standard Crank–Nicolson time discretization is combined with a second-order spatial approximation. The same applies to the simple finite element version of the scheme which is characterized by a lagging phase error due to the time discretization only. Note that this finite element scheme is equivalent to the scheme previously derived by Beam and Warming using a compact implicit approximation to the spatial derivative [25].

The relative phase errors of the Crank–Nicolson schemes are compared in Fig. 4.1 which shows that the phase response of both the finite difference and the standard finite element schemes deteriorates as v increases, whereas excellent phase speed and the unit CFL property at all wavelengths are obtained by the CNTG scheme. Therefore, in order to attain the unit CFL property in a nondissipative two-level scheme, the fourth-order spatial accuracy must be combined with a high-order time discretization belonging to the class of the canonical schemes devised for Hamiltonian systems [29]. The uniformity of the numerical performances of the CNTG scheme is further illustrated in Fig. 4.2 which compares the solutions to the problem (2.13) calculated by means of the three Crank–Nicolson schemes.

Note that for periodic boundary conditions the CNTG scheme, although unconditionally stable, cannot be operated for $v^2 \geqslant 1$ since the governing matrix in

TABLE IV

Modified Equations for the Schemes of Crank–Nicolson Type

Finite differences
$u_t + au_x = -\frac{1}{6}ah^2(1+\frac{1}{2}v^2)\,u_{xxx} - \frac{1}{120}ah^4(1+5v^2+\frac{3}{2}v^4)\,u_{xxxxx} + \cdots$
Finite elements
$u_t + au_x = -\frac{1}{12}ah^2v^2u_{xxx} + \cdots$
Taylor–Galerkin (finite elements)
$u_t + au_x = \frac{1}{720}ah^4(4-5v^2+v^4)\,u_{xxxxx} + \cdots$

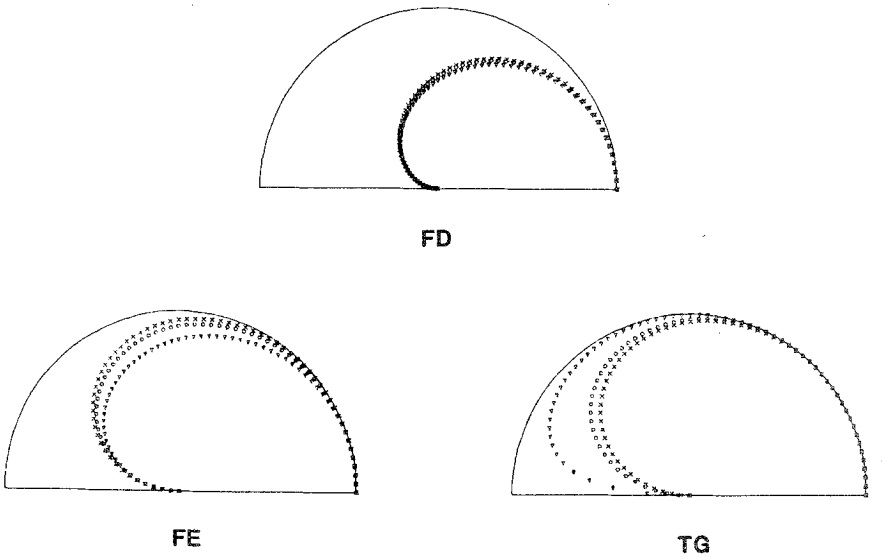

FIG. 4.1. Relative phase error ϕ^{CN}/ϕ^{ex} of the Crank–Nicolson schemes. (×) $\nu = 0.2$, (○) $\nu = 0.5$, (▽) $\nu = 0.9$.

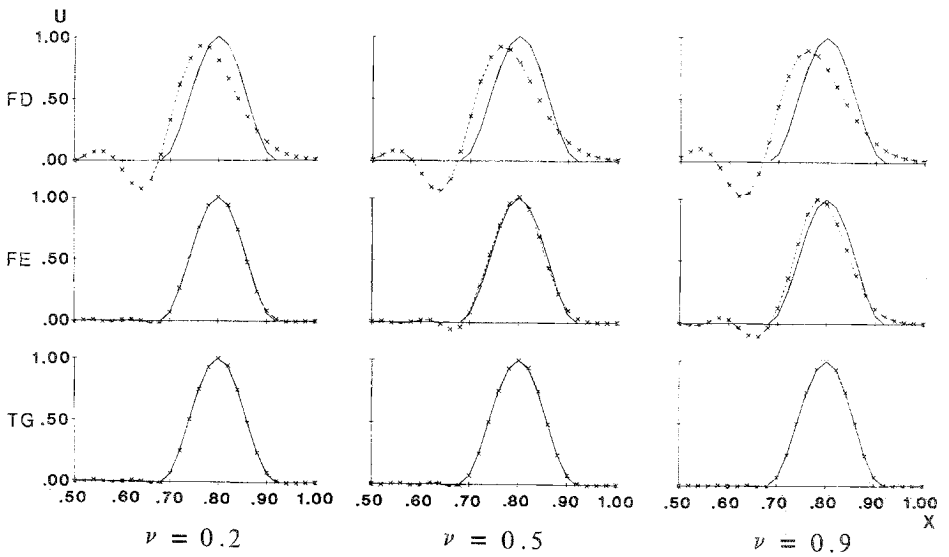

FIG. 4.2. Propagation of a cosine profile. Comparison of Crank–Nicolson schemes for several values of the Courant number.

Eq. (4.2) becomes singular, as shown by the detailed analysis of Harten and Tal-Ezer [27]. Furthermore, we have found oscillatory results for $v^2 \geqslant 1$ even in the case of the test problem (2.13) where nonperiodic boundary conditions are prescribed. This indicates that the CNTG scheme cannot be used safely for values of the Courant number exceeding unity.

5. Two-Dimensional Equations

This section extends the previous analysis to the case of two-dimensional equations in order to see to what extent the properties of the Taylor–Galerkin schemes in one dimension are still valid in the multidimensional case. This question has a certain interest considering the intrinsically multidimensional structure of finite element approximations as opposed to the direct product character of standard finite difference approximations to the spatial derivatives. The purely spatial discretization of the advection equation in two dimensions by finite differences and elements is first examined. Then, the fully discretized equations obtained using the Lax–Wendroff, leap-frog, and Crank–Nicolson time-stepping algorithms are considered. The domains of numerical stability for the two-dimensional schemes are determined. Some numerical comparisons between the finite difference and Taylor–Galerkin schemes are provided in the case of the Lax–Wendroff time-stepping. Furthermore, the effectiveness of the weak formulation in the treatment of outflow boundaries is illustrated by a simple two-dimensional example. Finally, the multidimensional wave equation will be examined to show the structure of the Lax–Wendroff Taylor–Galerkin scheme when the mathematical problem is formulated as a system of first-order hyperbolic equations.

5.1. *Spatial Semi-discretizations*

Consider the advection equation in two dimensions

$$u_t + \mathbf{a} \cdot \nabla u = 0, \tag{5.1}$$

where $\mathbf{a} = (a_x, a_y)$ is a constant velocity vector and $\nabla = (\partial/\partial x, \partial/\partial y)$. If one assumes an initial condition of the form $u(\mathbf{x}, 0) = u_0 e^{i\mathbf{p}\cdot\mathbf{x}}$, where $\mathbf{p} = (p_x, p_y)$ is the (dimensional) wavenumber vector, the exact solution to Eq. (5.1) is $u(\mathbf{x}, t) = u_0 e^{i(\mathbf{p}\cdot\mathbf{x} + \omega t)}$, where the exact frequency or phase velocity ω is defined simply by

$$\omega(\mathbf{p}, \mathbf{a}) = -\mathbf{a} \cdot \mathbf{p}. \tag{5.2}$$

A uniform rectangular mesh with sizes h_x and h_y in the two directions is introduced to discretize Eq. (5.1) spatially. Using standard second-order central differences, the semi-discrete version of Eq. (5.1),

$$\frac{dU}{dt} + \mathbf{c} \cdot \Delta U = 0, \tag{5.3}$$

is then obtained, where $U = U(t) = \{U_{j,k}(t),\ j, k = ..., -1, 0, 1, 2, ...\}$ is the vector of mesh-point values, $\mathbf{c} = (c, d) = (a_x/h_x, a_y/h_y)$ and $\Delta = (\Delta_x, \Delta_y)$ (the spatial difference operators Δ_x and Δ_y are defined in the Appendix). The phase velocity ω_{FD} associated with the semi-discrete finite difference equations (5.3) is found to be

$$\omega_{FD}(\xi, \mathbf{c}) = -c \sin \xi - d \sin \eta, \tag{5.4}$$

where $\xi = (\xi, \eta) = (h_x p_x, h_y p_y)$ is the dimensionless wave vector. To evaluate the properties of the spatial discretization in the two dimensional case, the velocity was

and the numerical phase velocity of waves propagating in this direction is then analyzed by considering $\xi = |\xi|\ (\cos \alpha, \sin \alpha)$. The ratio of the semi-discrete to the exact phase velocity is therefore given by the expression

$$r_{FD}(\xi, \mathbf{c}) = \frac{\omega_{FD}(\xi, \mathbf{c})}{\omega(\mathbf{p}, \mathbf{a})} = \frac{c \sin \xi + d \sin \eta}{\mathbf{c} \cdot \xi}, \tag{5.5}$$

which depends only on $|\xi|$ and α, $r_{FD} = r_{FD}(|\xi|, \alpha)$, in the case of a square mesh, $h_x = h_y = h$. As a consequence, the phase response displays a dependence on the wavelength $\lambda = 2\pi/|\mathbf{p}| = 2\pi h/|\xi|$ as well as on the direction α of propagation with respect to the mesh (anisotropy of the spatial discretization).

The use of a spatial semi-discretization by means of bilinear finite elements modifies the finite difference equations (5.3) in two respects:

(i) a more isotropic discretization of the operator ∇ is afforded, which is given by

$$\hat{\Delta} = (\hat{\Delta}_x, \hat{\Delta}_y) = \tfrac{2}{3}(\Delta_x + \tfrac{1}{4}\Delta_{xy} + \tfrac{1}{4}\Delta_{yx},\ \Delta_y + \tfrac{1}{4}\Delta_{xy} - \tfrac{1}{4}\Delta_{yx}); \tag{5.6}$$

(ii) the consistent mass matrix

$$M = 1 + \tfrac{1}{6}(\delta_x^2 + \delta_y^2 + \tfrac{1}{4}\delta_{xy}^2 + \tfrac{1}{4}\delta_{yx}^2) \tag{5.7}$$

is introduced to multiply the time derivative of the vector of nodal values $U(t)$, the first- and second-order operators Δ and δ^2 being defined in the Appendix.

The semi-discrete equations obtained by finite elements are therefore written as

$$M \frac{dU}{dt} + \mathbf{c} \cdot \hat{\Delta} U = 0. \tag{5.8}$$

Considering the Fourier transform of operators (5.6) and (5.7), one finds

$$\begin{aligned} \mathbf{c} \cdot \hat{\Delta}(\xi) &= \tfrac{2}{3}c[\sin \xi + \tfrac{1}{4}\sin(\xi + \eta) + \tfrac{1}{4}\sin(\xi - \eta)] \\ &\quad + \tfrac{2}{3}d[\sin \eta + \tfrac{1}{4}\sin(\xi + \eta) - \tfrac{1}{4}\sin(\xi - \eta)] \\ &= \tfrac{2}{3}c(1 + \tfrac{1}{2}\cos \eta)\sin \xi + \tfrac{2}{3}d(1 + \tfrac{1}{2}\cos \xi)\sin \eta, \end{aligned}$$

and

$$
\begin{aligned}
M(\xi) &= 1 - \tfrac{4}{9}(\sin^2 \tfrac{1}{2}\xi + \sin^2 \tfrac{1}{2}\eta) - \tfrac{1}{9}(\sin^2 \tfrac{1}{2}(\xi+\eta) + \sin^2 \tfrac{1}{2}(\xi-\eta)) \\
&= 1 - \tfrac{1}{3}[\tfrac{2}{3}(1-\cos\xi) + \tfrac{2}{3}(1-\cos\eta) + \tfrac{1}{3}(1-\cos\xi\cos\eta)] \\
&= \tfrac{2}{3}(1+\tfrac{1}{2}\cos\eta)[1-\tfrac{1}{3}(1-\cos\xi)] \\
&= \tfrac{2}{3}(1+\tfrac{1}{2}\cos\xi)[1-\tfrac{1}{3}(1-\cos\eta)].
\end{aligned}
$$

It follows that the phase velocity ω_{FE} associated with the semi-discrete finite element equations (5.8) has the form

$$
\omega_{\mathrm{FE}}(\xi, \mathbf{c}) = \frac{\mathbf{c}\cdot\hat{\boldsymbol{\Lambda}}(\xi)}{M(\xi)} = \frac{c\sin\xi}{1-(1/3)(1-\cos\xi)} + \frac{d\sin\eta}{1-(1/3)(1-\cos\eta)} \tag{5.9}
$$

which explicitly shows that the phase response of the one-dimensional semi-discretization is reproduced in the two-dimensional case for an advection velocity parallel to the mesh lines. In Fig. 5.1 the phase accuracy responses of different spatial discretizations are compared graphically by means of a polar representation (in the first quadrant) of the phase velocity ratio $r = r(|\xi|, \alpha)$, for different values of the wavelength $\lambda = 2\pi h/|\xi|$, as done in [4]. The finite difference discretization (5.5) is accurate only at long wavelengths and relatively anisotropic at small wavelengths. The use of finite elements for the representation of the advection

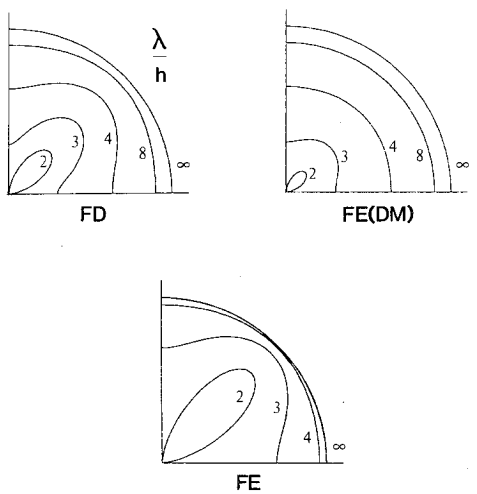

FIG. 5.1. Phase response of the semi-discrete approximations to the advection equation in two dimensions. Polar representation of the relative phase error for signals of a given wavelength, propagating in all directions. Comparison of spatial discretizations by central finite differences (upper left) and by bilinear finite elements with diagonalized mass matrix (upper right) and consistent mass matrix (lower). The quoted numbers indicate the value of the dimensionless wavelength λ/h.

(Eq. 5.6) combined with a diagonalized mass matrix reduces the anisotropy of the approximation even at small wavelengths without improving the propagation velocity of signals with long and intermediate wavelength. On the contrary, a finite element discretization including the consistent mass matrix (5.7) provides a very accurate and isotropic phase velocity except only for very short wavelengths.

5.2. *Lax–Wendroff Schemes*

To obtain fully discrete schemes of the Lax–Wendroff type for Eq. (5.1), the time discretization has to be analyzed before the process of spatial discretization. By means of the Taylor series (2.1), it is straightforward to obtain the multidimensional version of the Lax–Wendroff time-stepping algorithm in the form

$$(u^{n+1} - u^n)/\Delta t = -\mathbf{a} \cdot \nabla u^n + \tfrac{1}{2}\Delta t \mathbf{a} \cdot \nabla(\mathbf{a} \cdot \nabla u^n). \tag{5.10}$$

Therefore, in the multidimensional case, the stabilization of the Euler scheme is achieved by a second-order correction term which possess a tensorial character and acts only in the direction of the velocity and not transversely (streamline correction). When combined with standard finite differences, the algorithm gives the classical single-step Lax–Wendroff scheme in two dimensions [18],

$$\Delta U^{n+1}/\Delta t = -\mathbf{c} \cdot \Delta U^n + \tfrac{1}{2}\Delta t(c^2 \delta_x^2 + 2cd\, \Delta_x \Delta_y + d^2 \delta_y^2)\, U^n, \tag{5.11}$$

where $\Delta U^{n+1} = U^{n+1} - U^n$ and $U^n = \{U_{j,k}^n\}$. By introducing the Courant number vector $\boldsymbol{\nu} = (\nu, \mu) = \mathbf{c}\, \Delta t = (a_x \Delta t/h_x,\ a_y \Delta t/h_y)$, the LWFD scheme is written in the form

$$\Delta U^{n+1} = -\boldsymbol{\nu} \cdot \Delta U^n + \tfrac{1}{2}(\nu^2 \delta_x^2 + 2\nu\mu\, \Delta_x \Delta_y + \mu^2 \delta_y^2)\, U^n. \tag{5.12}$$

The amplification factor of the scheme (5.12) is

$$\begin{aligned} G_{\mathrm{FD}}^{\mathrm{LW}}(\xi, \boldsymbol{\nu}) = 1 &- [i\nu \sin \xi + \nu^2(1 - \cos \xi)] - \nu\mu \sin \xi \sin \eta \\ &- [i\mu \sin \eta + \mu^2(1 - \cos \eta)]. \end{aligned} \tag{5.13}$$

The domain of numerical stability in the plane (ν, μ) of the finite difference scheme (5.13) is obtained from the condition $|G_{\mathrm{FD}}^{\mathrm{LW}}(\xi, \boldsymbol{\nu})| \leqslant 1$ for all $\xi \in [0, \pi] \times [0, \pi]$ and is shown in Fig. 5.2. The reduced stability domain of the two-dimensional scheme with respect to that in one dimension is clearly seen. The largest time step for stability is found to be equal to that provided by the well-known condition $|\boldsymbol{\nu}| = |\mathbf{a}|\, \Delta t/h \leqslant 1/\sqrt{8}$ [30]. Note that another Lax–Wendroff scheme for the two-dimensional equation has also been considered by successively applying the one-dimensional Lax–Wendroff scheme (2.3) in the two cartesian directions, to give

$$\Delta U^{n+1} = -\boldsymbol{\nu} \cdot \Delta U^n + \tfrac{1}{2}\nu^2 \delta_x^2 U^n + \tfrac{1}{2}\mu^2 \delta_y^2 U^n.$$

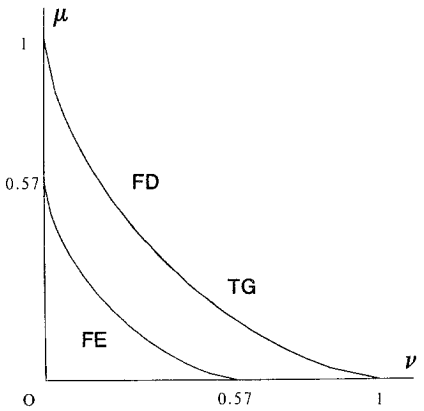

FIG. 5.2. Domains of numerical stability of the Lax–Wendroff schemes for the two-dimensional advection equation.

This direct-product scheme is, however, unstable and has led to the rediscovery of scheme (5.11) as the proper stabilization of the explicit Euler time-stepping in the two-dimensional case (tensor viscosity method) [31].

The use of bilinear finite elements with the time discretized equation (5.10) gives the LWFE scheme in two dimensions

$$M\,\Delta U^{n+1} = -\mathbf{v}\cdot\hat{\Delta}U^n + \tfrac{1}{2}(v^2\,\hat{\delta}_x^2 + 2v\mu\,\Delta_x\Delta_y + \mu^2\,\hat{\delta}_y^2)\,U^n, \tag{5.14}$$

with the difference operators $\hat{\Delta}$ and $\hat{\delta}$ given in the Appendix. It differs from the FD scheme (5.12) by the presence of the consistent mass matrix M and by a more isotropic representation of both the operator ∇ and the second-order operator $\mathbf{a}\cdot\nabla(\mathbf{a}\cdot\nabla)$. To obtain the TG version of the Lax–Wendroff scheme, Eq. (5.10) has to be replaced by

$$[1 - \tfrac{1}{6}(\Delta t)^2\,\mathbf{a}\cdot\nabla(\mathbf{a}\cdot\nabla)](u^{n+1}-u^n)/\Delta t = -\mathbf{a}\cdot\nabla u^n + \tfrac{1}{2}\,\Delta t\,\mathbf{a}\cdot\nabla(\mathbf{a}\cdot\nabla u^n). \tag{5.15}$$

After the spatial discretization using bilinear elements, Eq. (5.15) becomes

$$M_g\,\Delta U^{n+1} = -\mathbf{v}\cdot\hat{\Delta}U^n + \tfrac{1}{2}(v^2\,\hat{\delta}_x^2 + 2v\mu\,\Delta_x\Delta_y + \mu^2\,\hat{\delta}_y^2)\,U^n, \tag{5.16}$$

where the generalized mass matrix M_g is defined by

$$M_g = M - \tfrac{1}{6}(v^2\,\hat{\delta}_x^2 + 2v\mu\,\Delta_x\Delta_y + \mu^2\,\hat{\delta}_y^2). \tag{5.17}$$

Note that the corrective term in M_g has the same tensorial structure as the second-order correction term in Eq. (5.14). The amplification factor of the two-dimensional LWTG scheme is

$$G_{\mathrm{TG}}^{\mathrm{LW}}(\xi, \mathbf{v}) = 1 - M_g^{-1}(\xi, \mathbf{v})[A(\xi, \mathbf{v}) - \tfrac{1}{2}K(\xi, \mathbf{v})], \tag{5.18}$$

where

$$M_g(\xi, \nu) = M(\xi) - \tfrac{1}{6}K(\xi, \nu), \tag{5.18a}$$

$$A(\xi, \nu) = \tfrac{2}{3}i\nu(1 + \tfrac{1}{2}\cos\eta)\sin\xi + \tfrac{2}{3}i\mu(1 + \tfrac{1}{2}\cos\xi)\sin\eta, \tag{5.18b}$$

$$K(\xi, \nu) = \tfrac{4}{3}\nu^2(1 + \tfrac{1}{2}\cos\eta)(1 - \cos\xi) + 2\nu\mu\sin\xi\sin\eta + \tfrac{4}{3}\mu^2(1 + \tfrac{1}{2}\cos\xi)(1 - \cos\eta). \tag{5.18c}$$

The stability domains of the FE and TG Lax–Wendroff schemes in two-dimensions are shown in Fig. 5.2. As in the one-dimensional case, the simplistic FE scheme has a stability domain smaller than that of the FD method whereas the TG scheme has the same stability range as the FD method. The exact coincidence of the two curves was not recognized by the authors in [11] due to a lack of spatial resolution in the ξ plane.

The phase properties of the three schemes are compared in Fig. 5.3 which

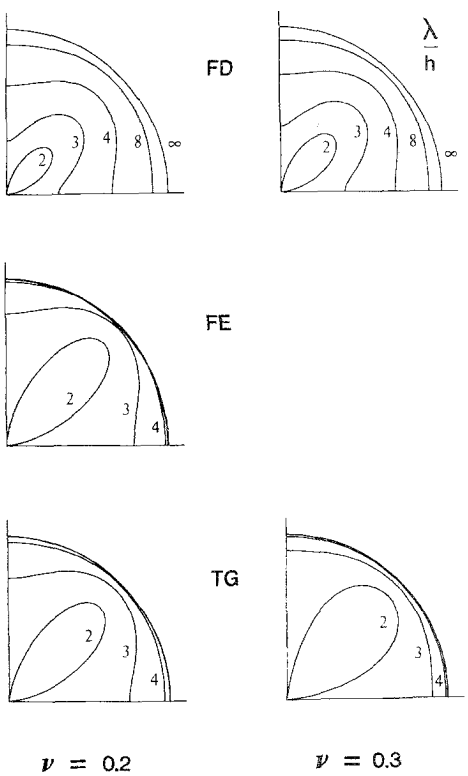

FIG. 5.3. Phase velocity error of the Lax–Wendroff schemes for the advection equation in two dimensions.

provides a polar representation of the phase velocity error of the fully discrete equations defined as

$$r^{\mathrm{LW}}(\xi, \nu) = \frac{\phi^{\mathrm{LW}}(\xi, \nu)}{\phi^{\mathrm{ex}}(\xi, \nu)} = \frac{\arg(G^{\mathrm{LW}}(\xi, \nu))}{-\nu \cdot \xi}. \tag{5.19}$$

The two values $|\nu| = 0.2$ and $|\nu| = 0.3$ have been considered. The response of both FD and TG schemes improves as $|\nu|$ increases. The superior phase accuracy of the finite element spatial discretization is seen to hold irrespectively of the direction of propagation of the waves.

To compare the two-dimensional Lax–Wendroff schemes considered so far, the advection of a product-cosine hill in a pure rotation velocity field is considered. The initial condition is

$$u_0(\mathbf{x}) = \begin{cases} \frac{1}{4}[1 + \cos \pi X][1 + \cos \pi Y] & \text{if } X^2 + Y^2 \leqslant 1 \\ 0 & \text{if } X^2 + Y^2 \geqslant 1, \end{cases}$$

where $\mathbf{X} = (\mathbf{x} - \mathbf{x}_0)/\sigma$, $\mathbf{x}_0$ and σ being the initial position of the centre and the radius of the cosine hill. The advection field is a pure rotation with unit angular velocity, namely $\mathbf{a}(\mathbf{x}) = (-y, x)$, so that a nonconstant coefficient linear equation is solved for which Eq. (5.15) is still valid provided $\mathbf{a}$ is interpreted as $\mathbf{a} = \mathbf{a}(\mathbf{x})$.

For the treatment of the boundary conditions, it is necessary to split Γ in the two parts Γ_{in} and Γ_{out} (see Fig. 5.4) defined by

$$\mathbf{n} \cdot \mathbf{a}|_{\Gamma_{\mathrm{in}}} < 0 \qquad \text{and} \qquad \mathbf{n} \cdot \mathbf{a}|_{\Gamma_{\mathrm{out}}} \geqslant 0. \tag{5.20}$$

In this case, the value of the unknown u is prescribed along Γ_{in} whereas no boundary condition is prescribed on Γ_{out} [32]. Correspondingly, the weighting functions w are chosen to satisfy the homogeneous boundary condition on Γ_{in}, $w|_{\Gamma_{\mathrm{in}}} = 0$, but $w|_{\Gamma_{\mathrm{out}}} \neq 0$. Thus, when the weak form of Eq. (5.15) is derived using the integration

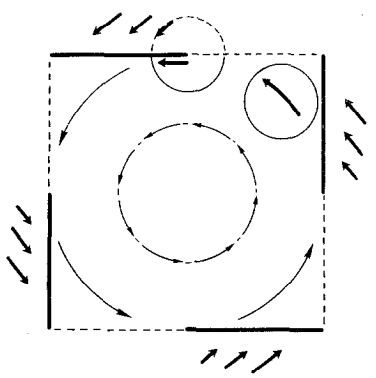

FIG. 5.4. Computational domain and boundary for the problem of a cosine hill advected by a pure rotation velocity field.

by parts (Green–Gauss theorem) one has to retain the surface integrals over Γ

as

$$\langle w, \Delta u^{n+1}\rangle/\Delta t + \tfrac{1}{6}\Delta t\{\langle \nabla\cdot(w\mathbf{a}), \mathbf{a}\cdot\nabla\,\Delta u^{n+1}\rangle - \int_{\Gamma_{\text{out}}} w\mathbf{n}\cdot\mathbf{a}\;\mathbf{a}\cdot\nabla\,\Delta u^{n+1}\,d\Gamma\}$$

$$= -\langle w, \mathbf{a}\cdot\nabla u^n\rangle - \tfrac{1}{2}\Delta t\left\{\langle \nabla\cdot(w\mathbf{a}), \mathbf{a}\cdot\nabla u^n\rangle - \int_{\Gamma_{\text{out}}} w\mathbf{n}\cdot\mathbf{a}\;\mathbf{a}\cdot\nabla u^n\,d\Gamma\right\}, \qquad (5.21)$$

where in general $\mathbf{a} = \mathbf{a}(\mathbf{x})$.

A uniform mesh of 30×30 quadrilateral elements over the unit square $[-\frac{1}{2}, \frac{1}{2}]\times[-\frac{1}{2}, \frac{1}{2}]$ has been employed in the calculations. The numerical solutions for the case $\mathbf{x}_0 = (\frac{1}{6}, \frac{1}{6})$, $\sigma = 0.2$ are shown in Fig. 5.5 after a complete revolution for two time-step values, $\Delta t = 2\pi/200$ and $\Delta t = 2\pi/120$. To compare the accuracy of the various

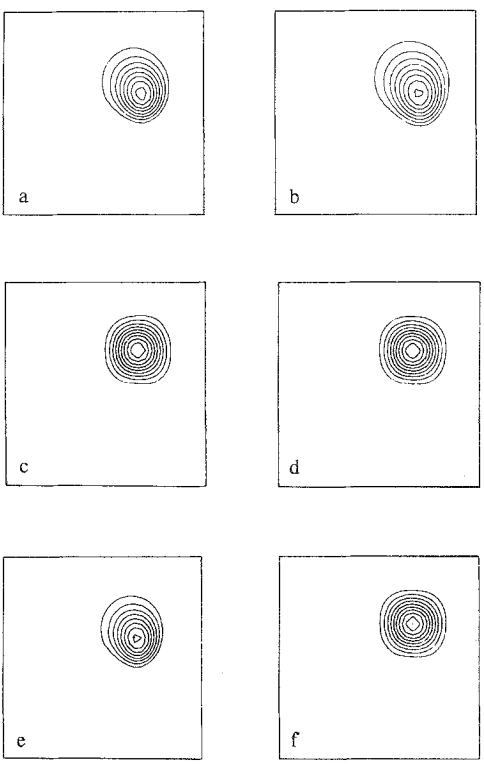

FIG. 5.5. Advection of a cosine hill in a pure rotation velocity field. Comparison of the numerical solutions after a complete revolution calculated by means of the LW schemes with $\Delta t = 2\pi/200$. (a) FD, $U_{\max} = 0.852$, $U_{\min} = -0.167$, err $= 0.246$, (b) FE(DM), $U_{\max} = 0.818$, $U_{\min} = -0.177$, err $= 0.328$, (c) FE, $U_{\max} = 0.987$, $U_{\min} = -0.016$, err $= 0.0020$, (d) TG, $U_{\max} = 0.988$, $U_{\min} = -0.022$, err $= 0.0016$. With $\Delta t = 2\pi/120$, (e) FD, $U_{\max} = 0.826$, $U_{\min} = -0.162$, err $= 0.262$, (f) TG, $U_{\max} = 0.978$, $U_{\min} = -0.020$, err $= 0.0020$.

schemes, the maximum and minimum values of the computed solutions are provided together with the corresponding L^2-error defined by $\text{err} = \|U-u\|/\|u\|$, where $\|u\|^2 = \sum_j [u(\mathbf{x}_j)]^2$. The greater accuracy of the schemes with the consistent or generalized mass matrix is clearly seen. Admittedly, they are computationally more expensive than the explicit FD scheme because at each time step the solution of a banded (symmetric) linear system is required. The inversion of the mass matrix can, however, be approximated by a purely explicit iterative technique which takes a particularly simple form due to the incremental character of the equations [13]. In the case of linear equations, two iterations are found to be sufficient to preserve the phase accuracy at all the relevant wavelengths. For nonlinear problems, three iterations are to be used, particularly in the case of the TG scheme where a different generalized mass matrix is generated at each time step.

In the above problem the initial condition is such that the rotating hill does not reach the boundary so that the numerical results are insensitive to the boundary conditions actually used. To assess the influence on the solution accuracy of properly accounting for the surface integrals on outflow boundaries, a second test case has been undertaken using $\mathbf{x}_0 = (0.3, 0.3)$ and $\sigma = 0.2$ so that the cosine hill "interacts" with the boundary. The solutions provided by the LWTG scheme with $\Delta t = 2\pi/200$ at different times are shown in Fig. 5.6. The numerical errors are found to be approximately twice those in the previous example where the hill always remains inside the computational domain. This indicates that the variationally generated surface integrals in Eq. (5.21) ensure a very low level of spurious reflections at outflow boundaries.

5.3. *Leap-Frog Schemes*

By generalizing the second- and fourth-order accurate leap-frog algorithms to the multidimensional case, it is straightforward to obtain the LFFD and LFTG schemes for the advection equation (5.1), in the forms

$$U^{n+1} - U^{n-1} = -2\mathbf{v}\cdot\Delta U^n \tag{5.22}$$

and

$$M_g(U^{n+1} - U^{n-1}) = -2\mathbf{v}\cdot\hat{\Delta} U^n, \tag{5.23}$$

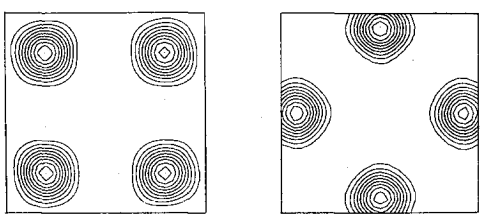

FIG. 5.6. Advection of a cosine hill in the presence of inflow and outflow boundaries. Numerical solution at different times calculated by means of LWTG scheme with $\Delta t = 2\pi/200$. After one complete revolution $U_{\max} = 0.953$, $U_{\min} = -0.024$, $\text{err} = 0.00359$.

where $\hat{\Delta}$ and M_g are defined by Eqs. (5.6) and (5.17), respectively. The LFFE scheme is obtained from the LFTG scheme by simply replacing the generalized mass matrix M_g with the consistent mass matrix M.

The stability analysis of the two-dimensional leap-frog schemes leads to the domains of numerical stability in the plane (ν, μ) depicted in Fig. 5.7. With respect to the Lax–Wendroff schemes, one notes that the TG scheme is more unstable than the FD method. On the other hand, by comparing the two TG schemes, the leap-frog differencing guarantees a greater stability domain than the Lax–Wendroff time descretization. The phase velocity error of the three fully discrete leap-frog schemes are shown in Fig. 5.8 by the polar representation diagrams for $|\mathbf{v}| = 0.3$ and $|\mathbf{v}| = 0.6$. One notes the anomalous behaviour of the FE scheme with lagging or leading phase errors depending on the wave propagation direction. Such an effect disappears in the TG scheme. Furthermore, one observes that in both the FD and the TG scheme, as $|\mathbf{v}|$ tends to the stability limit, the phase velocity of waves propagating parallel to the mesh tends to the exact value only for wavelengths $\lambda = 2\pi h/|\xi| \geqslant 4h$, in conformity with the one-dimensional case.

5.4. *Crank–Nicolson Schemes*

Similarly, from the Crank–Nicolson time-stepping algorithms, the two-dimensional version of the CNFD and CNTG schemes is obtained in the incremental forms

$$[1 + \tfrac{1}{2}\mathbf{v} \cdot \Delta](U^{n+1} - U^n) = -\mathbf{v} \cdot \Delta U^n, \tag{5.24}$$

$$[\bar{M}_g + \tfrac{1}{2}\mathbf{v} \cdot \hat{\Delta}](U^{n+1} - U^n) = -\mathbf{v} \cdot \hat{\Delta} U^n, \tag{5.25}$$

where

$$\bar{M}_g = M + \tfrac{1}{12}(\nu^2 \delta_x^2 + 2\nu\mu \Delta_x \Delta_y + \mu^2 \delta_y^2). \tag{5.25'}$$

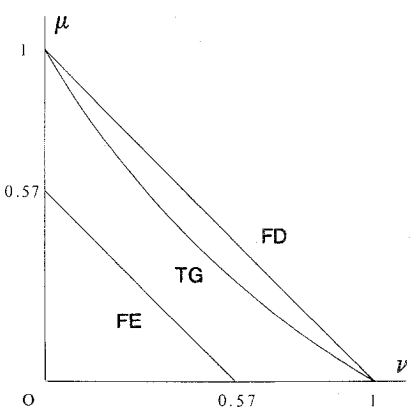

FIG. 5.7. Domains of numerical stability of the leap-frog schemes for the two-dimensional advection equation.

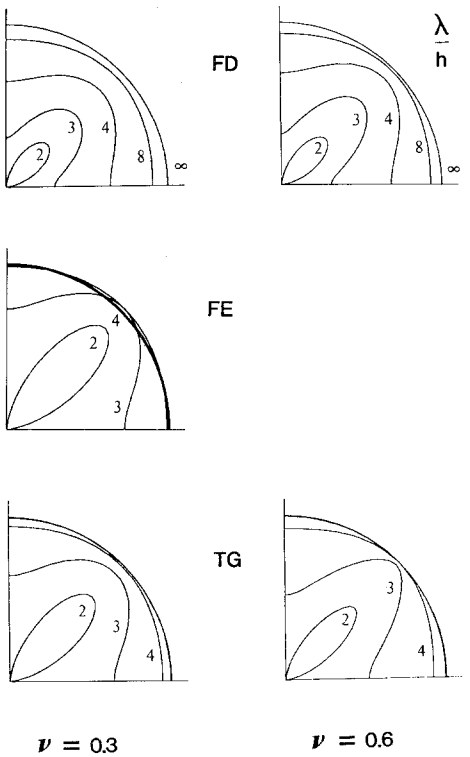

FIG. 5.8. Polar representation of the phase velocity error of the leap-frog schemes for the advection equation in two dimensions.

Again, the simple FE scheme is obtained from the TG one by replacing $\bar{M}_g$ with M. In all cases $|G^{CN}| = 1$ and the Crank–Nicolson schemes are unconditionally stable. In Fig. 5.9 the phase response of the two-dimensional schemes for waves propagating in all directions and for the two values $|\mathbf{v}| = 0.3$ and $|\mathbf{v}| = 0.9$ are represented graphically by polar diagrams. Whereas the accuracy of both the FD and FE schemes decreases as $|\mathbf{v}|$ increases, the CNTG scheme tends to reproduce the exact phase velocity as $|\mathbf{v}| \to 1$, almost uniformly for all propagation directions (nearly isotropic unit CFL property). This behaviour is more clearly illustrated in Fig. 5.10 which shows the phase velocity diagrams for some limiting values of $|\mathbf{v}|$ as $|\mathbf{v}| \to 1$. Note that the singularity of the phase error at $|\mathbf{v}| = 1$ discovered by Harten and Tal-Ezer in the one-dimensional case [27] is also found in two dimensions, as was indeed expected.

5.5. *Wave equation*

In this subsection, the multidimensional wave equation is considered and discretized by the Lax–Wendroff scheme just for the purpose of showing how the structure of the Lax–Wendroff correction term depends on the vector character as

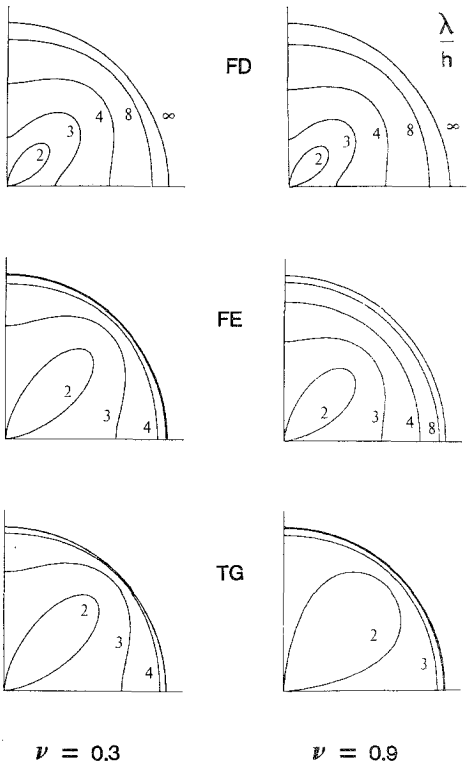

FIG. 5.9. Phase velocity error of the Crank–Nicolson schemes for the advection equation in two dimensions.

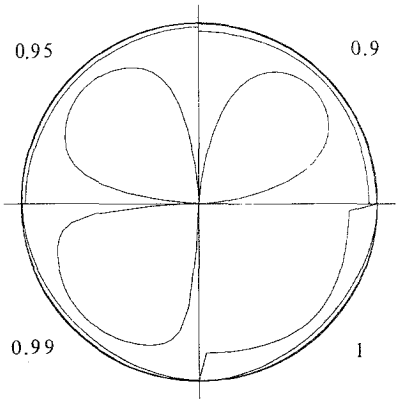

FIG. 5.10. Phase velocity error of the Crank–Nicolson Taylor–Galerkin scheme.

well as on the spatial dimensionality of the system of hyperbolic equations. Consider the linear equation governing the propagation of longitudinal waves in two dimensions

$$\psi_{tt} = a^2 \nabla^2 \psi, \tag{5.26}$$

where ∇^2 is the two-dimensional Laplacian operator. Since $\nabla^2\psi = \nabla \cdot \nabla\psi$, the introduction of the two unknowns $v = \psi_t$ and $\mathbf{w} = -a\nabla\psi$ allows the expression of Eq. (5.26) as a system of first-order hyperbolic equations

$$\begin{aligned} v_t &= -a \nabla \cdot \mathbf{w}, \\ \mathbf{w}_t &= -a \nabla v. \end{aligned} \tag{5.27}$$

By introducing the three-component vector unknown $u = (v, \mathbf{w}) = (v, w_1, w_2)$, system (5.27) can be rewritten as

$$u_t = a \nabla_* u, \tag{5.28}$$

$$\nabla_* = \begin{bmatrix} 0 & \nabla \\ \nabla^{\mathrm{T}} & O \end{bmatrix}. \tag{5.29}$$

It is straightforward to derive the third-order Lax–Wendroff time discretization (5.15) for system (5.28). By simple calculation one obtains

$$[1 - \tfrac{1}{6}(\Delta t)^2 a^2 (\nabla_*)^2](u^{n+1} - u^n)/\Delta t = -a \nabla_* u^n + \tfrac{1}{2}\Delta t a^2 (\nabla_*)^2 u^n, \tag{5.30}$$

where the second-order operator $(\nabla_*)^2$ is given by

$$(\nabla_*)^2 = \begin{bmatrix} \nabla^2 & \mathbf{0} \\ \mathbf{0}^{\mathrm{T}} & \nabla(\nabla \cdot) \end{bmatrix}. \tag{5.31}$$

The coupling structure engendered by the operator $(\nabla_*)^2$ is made explicit by considering the weak form of Eq. (5.30) with a separate representation of the equations for the components v and $\mathbf{w}$ of the unknown u. The weak equation for the scalar unknown v is

$$\langle z, \Delta v^{n+1} \rangle / \Delta t + \tfrac{1}{6}\Delta t a^2 \langle \nabla z, \nabla \Delta v^{n+1} \rangle = -a \langle z, \nabla \cdot \mathbf{w}^n \rangle - \tfrac{1}{2}\Delta t a^2 \langle \nabla z, \nabla v^n \rangle, \tag{5.32}$$

whereas that for the vector unknown $\mathbf{w}$ is

$$\langle \mathbf{y}, \Delta \mathbf{w}^{n+1} \rangle / \Delta t + \tfrac{1}{6}\Delta t a^2 \langle \nabla \cdot \mathbf{y}, \nabla \cdot \Delta \mathbf{w}^{n+1} \rangle = -a \langle \mathbf{y}, \nabla v^n \rangle - \tfrac{1}{2}\Delta t a^2 \langle \nabla \cdot \mathbf{y}, \nabla \cdot \mathbf{w}^n \rangle, \tag{5.33}$$

where the incremental unknowns $\Delta v^{n+1} = v^{n+1} - v^n$ and $\Delta \mathbf{w}^{n+1} = \mathbf{w}^{n+1} - \mathbf{w}^n$ have been introduced. One notes that the second-order and third-order correction terms leave the scalar unknown decoupled from the vector one, but introduce a coupling between the two components w_1 and w_2 of the vector unknown $\mathbf{w}$.

6. Conclusion

The paper has investigated the causes of the numerical difficulties encountered in the solution of hyperbolic problems when classical, second-order accurate, time-marching methods are coupled to piecewise linear approximations on a fixed mesh. An analysis based on the modified equation method has pointed out that the proper remedy to overcome the above difficulties consists of extending the Taylor series in the time increment to the third order *before* discretizing spatially by means of the conventional Galerkin formulation. This procedure is not common in the finite element approach to evolution problems wherein the spatial approximation usually precedes the temporal discretization.

On the contrary, the reversed order of the two discretizations (time–space) considered in the paper leads to highly accurate and compact Taylor–Galerkin schemes for solving hyperbolic equations, which may be regarded as the proper generalization to finite elements of the Lax–Wendroff, leap-frog, and Crank–Nicolson finite difference methods. Surprisingly enough, the simple argument which has led Lax and Wendroff to formulate their celebrated finite difference scheme is found to be capable of upgrading all three second-order accurate time integrators so as to ensure a proper matching with a finite-element-based spatial approximation. Furthermore, the resulting Taylor–Galerkin schemes appear quite naturally in the so-called incremental (delta) form and are characterized by the absence of any adjustable parameter. In this latter respect, an important result of the present analysis has been the elimination of the need for free or adjustable parameters as encountered in Petrov–Galerkin schemes for hyperbolic equations. Therefore, the present work appears to complement for transient hyperbolic problems the recent work of Ortiz on the steady advection–diffusion equation [33] in which a variational formulation of the advection–diffusion boundary value problem was introduced, leading to a parameter-free Petrov–Galerkin method for steady problems.

As far as nonlinear problems are concerned, Cullen and Morton [7] have shown that the high spatial accuracy of the Galerkin finite element formulation also holds for hyperbolic equations with quadratic nonlinearities. It follows that the Taylor–Galerkin schemes studied herein can be generalized to deal with problems in this class. This possibility has already been investigated in [11] where encouraging results have been obtained.

Finally, the Taylor–Galerkin methodology discussed in the present paper may also find applications in the numerical solution of parabolic equations. This has been suggested in [14], where the solution of mixed advection–diffusion problems is considered.

APPENDIX: Spatial Difference Operators in Two Dimensions

The elementary difference operators used in Section 5 to approximate the spatial derivative $\nabla = (\partial/\partial x,\ \partial/\partial y)$ by central finite differences and by bilinear finite elements are defined as

$$(\Delta_x U)_{j,k} = \tfrac{1}{2}(U_{j+1,k} - U_{j-1,k})$$
$$(\Delta_y U)_{j,k} = \tfrac{1}{2}(U_{j,k+1} - U_{j,k-1})$$

$$(\Delta_{xy} U)_{j,k} = \tfrac{1}{2}(U_{j+1,k+1} - U_{j-1,k-1})$$
$$(\Delta_{yx} U)_{j,k} = \tfrac{1}{2}(U_{j+1,k-1} - U_{j-1,k+1})$$

$$\hat{\Delta}_x = \tfrac{2}{3}(\Delta_x + \tfrac{1}{4}\Delta_{xy} + \tfrac{1}{4}\Delta_{yx})$$
$$\hat{\Delta}_y = \tfrac{2}{3}(\Delta_y + \tfrac{1}{4}\Delta_{xy} - \tfrac{1}{4}\Delta_{yx}).$$

Hereafter, we also list the second-order difference operators used in Section 5 to represent the differential operator $\mathbf{a}\cdot\nabla(\mathbf{a}\cdot\nabla)$ in two dimensions by finite differences and to represent the consistent mass matrix and the operator $\mathbf{a}\cdot\nabla(\mathbf{a}\cdot\nabla)$ by bilinear finite elements

$$(\delta_x^2 U)_{j,k} = U_{j+1,k} - 2U_{j,k} + U_{j-1,k}$$
$$(\delta_y^2 U)_{j,k} = U_{j,k+1} - 2U_{j,k} + U_{j,k-1}$$

$$(\delta_{xy}^2 U)_{j,k} = U_{j+1,k+1} - 2U_{j,k} + U_{j-1,k-1}$$
$$(\delta_{yx}^2 U)_{j,k} = U_{j+1,k-1} - 2U_{j,k} + U_{j-1,k+1}$$

$$\hat{\delta}_x^2 = \tfrac{2}{3}\delta_x^2 - \tfrac{1}{3}\delta_y^2 + \tfrac{1}{6}(\delta_{xy}^2 + \delta_{yx}^2)$$
$$\hat{\delta}_y^2 = \tfrac{2}{3}\delta_y^2 - \tfrac{1}{3}\delta_x^2 + \tfrac{1}{6}(\delta_{xy}^2 + \delta_{yx}^2).$$

Acknowledgments

The authors are grateful to the reviewers for their useful comments and suggestions.

References

1. R. D. Richtmyer and K. W. Morton, *Difference Methods for Initial-Value Problems* (Wiley, New York, 1967).
2. P. J. Roache, *Computational Fluid Dynamics* (Hermosa, Albuquerque, 1972).
3. D. A. Anderson, J. C. Tannehill, and R. H. Pletcher, *Computational Fluid Mechanics and Heat Transfer* (Hemisphere, Washington, 1984).
4. R. Vichnevetsky and J. B. Bowles, *Fourier Analysis of Numerical Approximations of Hyperbolic Equations* (SIAM, Philadelphia, 1982).

5. P. M. GRESHO, R. L. LEE, AND R. SANI, in *Finite Elements in Fluids* **3**, 325 (1978).
6. A. J. BAKER AND M. O. SOLIMAN, *J. Comput. Phys.* **32**, 289 (1979).
7. M. J. P. CULLEN AND K. W. MORTON, *J. Comput. Phys.* **34**, 245 (1980).
8. K. W. MORTON AND A. K. PARROTT, *J. Comput. Phys.* **36**, 249 (1980).
9. K. W. MORTON, *Comput. Meth. Appl. Mech. Eng.* **52**, 847 (1985).
10. J. DONEA, *Int. J. Numer. Methods. Eng.* **20**, 101 (1984).
11. V. SELMIN, J. DONEA, AND L. QUARTAPELLE, *Comput. Methods Appl. Mech. Eng.* **52**, 817 (1985).
12. V. SELMIN, J. DONEA, AND L. QUARTAPELLE, in *Proceedings of the International Conference on Numerical Methods for Transient and Coupled Problems, Venice, Italy, 1984*, edited by P. Bettess *et al.* (Pineridge, Swansea, 1984), p. 816.
13. J. DONEA, S. GIULIANI, AND J.-P. HALLEUX, in *Proceedings of the International Conference on Numerical Methods for Non-Linear Problems, Barcelona, Spain, 1984*, edited by C. Taylor *et al.* (Pineridge, Swansea, 1984), p. 123.
14. J. DONEA, S. GIULIANI, H. LAVAL, AND L. QUARTAPELLE, *Comput. Methods Appl. Mech. Eng.* **45**, 123 (1984).
15. R. F. WARMING AND B. J. HYETT, *J. Comput. Phys.* **14**, 159 (1974).
16. R. LISKA, *Comput. Phys. Comm.* **34**, 175 (1984).
17. T. F. CHAN, *SIAM J. Numer. Anal.* **21**, 272 (1984).
18. P. D. LAX AND B. WENDROFF, *Commun. Pure Appl. Math.* **13**, 217 (1960).
19. I. CHRISTIE, D. F. GRIFFITHS, A. R. MITCHELL, AND O. C. ZIENKIEWICZ, *Int. J. Numer. Methods Eng.* **10**, 1389 (1976).
20. D. W. KELLY, S. NAKAZAWA, O. C. ZIENKIEWICZ, AND J. C. HEINRICH, *Int. J. Numer. Methods Eng.* **15**, 1705 (1980).
21. T. J. R. HUGHES AND A. BROOKS, *Finite Elements in Fluids* **4**, 47 (1982).
22. D. B. DUNCAN AND D. F. GRIFFITHS, *Comput. Methods Appl. Mech. Eng.* **45**, 147 (1984).
23. H. O. KREISS AND J. OLIGER, *Tellus* **24**, 199 (1972).
24. B. ENGQUIST AND H. O. KREISS, *Comput. Methods Appl. Mech. Eng.* **17/18**, 581 (1979).
25. R. M. BEAM AND R. F. WARMING, *J. Comput. Phys.* **22**, 87 (1976).
26. A. HARTEN AND H. TAL-EZER, *Math. Comput.* **36**, 353 (1981).
27. A. HARTEN AND H. TAL-EZER, *J. Comput. Phys.* **41**, 329 (1981).
28. A. ISERLES AND G. STRANG, *Trans. Amer. Math. Soc.* **277**, 779 (1983).
29. K. FENG, Symplectic Geometry and Numerical Methods in Fluid Dynamics, in *Proceedings of the Tenth International Conference on Numerical Methods in Fluid Dynamics, Beijing, China, 1986* (Springer-Verlag, Berlin, 1986).
30. E. TURKEL, *J. Comput. Phys.* **15**, 226 (1974).
31. J. K. DUKOWICZ AND J. D. RAMSHAW, *J. Comput. Phys.* **32**, 71 (1979).
32. G. J. FIX, *SIAM J. Appl. Math.* **29**, 371 (1975).
33. M. ORTIZ, *Int. J. Eng. Sci.* **23**, 717 (1985).